Do gravel bed river size distributions record channel network structure?

Leonard S. Sklar,[1] William E. Dietrich,[2] Efi Foufoula-Georgiou,[3] Bruno Lashermes,[3] and Dino Bellugi[2]

Received 13 March 2006; revised 21 April 2006; accepted 26 April 2006; published 24 June 2006.

[1] Bed load sediment particles supplied to channels by hillslopes are reduced in size by abrasion during downstream transport. The branching structure of the channel network creates a distribution of downstream travel distances to a given reach of river and thus may strongly influence the grain size distribution of the long-term bed load flux through that reach. Here we investigate this hypothesis, using mass conservation and the Sternberg exponential decay equation for particle abrasion, to predict bed material variability at multiple scales for both natural and artificial drainage networks. We assume that over a sufficiently long timescale, no net deposition occurs and that grains less than 2 mm are swept away in suspension. We find that abrasion during fluvial transport has a surprisingly small effect on the bed load sediment grain size distribution, for the simple case of spatially uniform supply of poorly sorted hillslope sediments. This occurs because at any point in the channel network, local resupply offsets the size reduction of material transported from upstream. Thus river bed material may essentially mirror the coarse component of the size distribution of hillslope sediment supply. Furthermore, there is a predictable distance downstream at which the bed load grain size distribution reaches a steady state. In the absence of net deposition due to selective transport, large-scale variability in bed material, such as downstream fining, must then be due primarily to spatial gradients in hillslope sediment production and transport characteristics. A second key finding is that average bed load flux will tend to stabilize at a constant value, independent of upstream drainage area, once the rate of silt production by bed load abrasion per unit travel distance is equal to the rate of coarse sediment supply per unit channel length (q). Bed load flux equilibrates over a distance that scales with the inverse of the fining coefficient in the abrasion rate law (α) and can be approximated simply as $q/3\alpha$. Thus the efficiency of particle abrasion sets a fundamental length scale, shorter for weaker rocks and longer for harder rocks, which controls the expression in the river bed of variability in sediment supply. We explore the role of the abrasion length scale in modulating the influence of sediment supply variability in a number of channel network contexts, including individual tributary junctions, a sequence of tributary inputs along a main stem channel, and variable basin shapes and network architecture as expressed by the width function. These findings highlight the need for both data and theory that can be used to predict the grain size distributions supplied to channels by hillslopes.

Citation: Sklar, L. S., W. E. Dietrich, E. Foufoula-Georgiou, B. Lashermes, and D. Bellugi (2006), Do gravel bed river size distributions record channel network structure?, *Water Resour. Res.*, *42*, W06D18, doi:10.1029/2006WR005035.

1. Introduction

[2] The self-organized pattern of a river network creates a hierarchical structure of channel pathways down which runoff and the sediment waste from hillslopes travels. Much has been written about the fractal characteristics of river networks [e.g., *Rodriguez-Iturbe and Rinaldo*, 1997], of the incoming precipitation that drives landscape erosion and channel incision [e.g., *Venugopal et al.*, 2006], and of the resulting runoff characteristics that record the integral of precipitation and runoff paths [e.g., *Gupta et al.*, 1996; *Menabde and Sivapalan*, 2001; *Dodov and Foufoula-Georgiou*, 2005; *Troutman and Over*, 2001]. There are other possible scaling relationships associated with the introduction and passage of sediment down through the networks. Sediment entering rivers is typically very poorly sorted and arrives episodically both spatially and through

[1]Department of Geosciences, San Francisco State University, San Francisco, California, USA.
[2]Department of Earth and Planetary Science, University of California, Berkeley, California, USA.
[3]St. Anthony Falls Laboratory and Department of Civil Engineering, University of Minnesota–Twin Cities, Minneapolis, Minnesota, USA.

0043-1397/06/2006WR005035$09.00

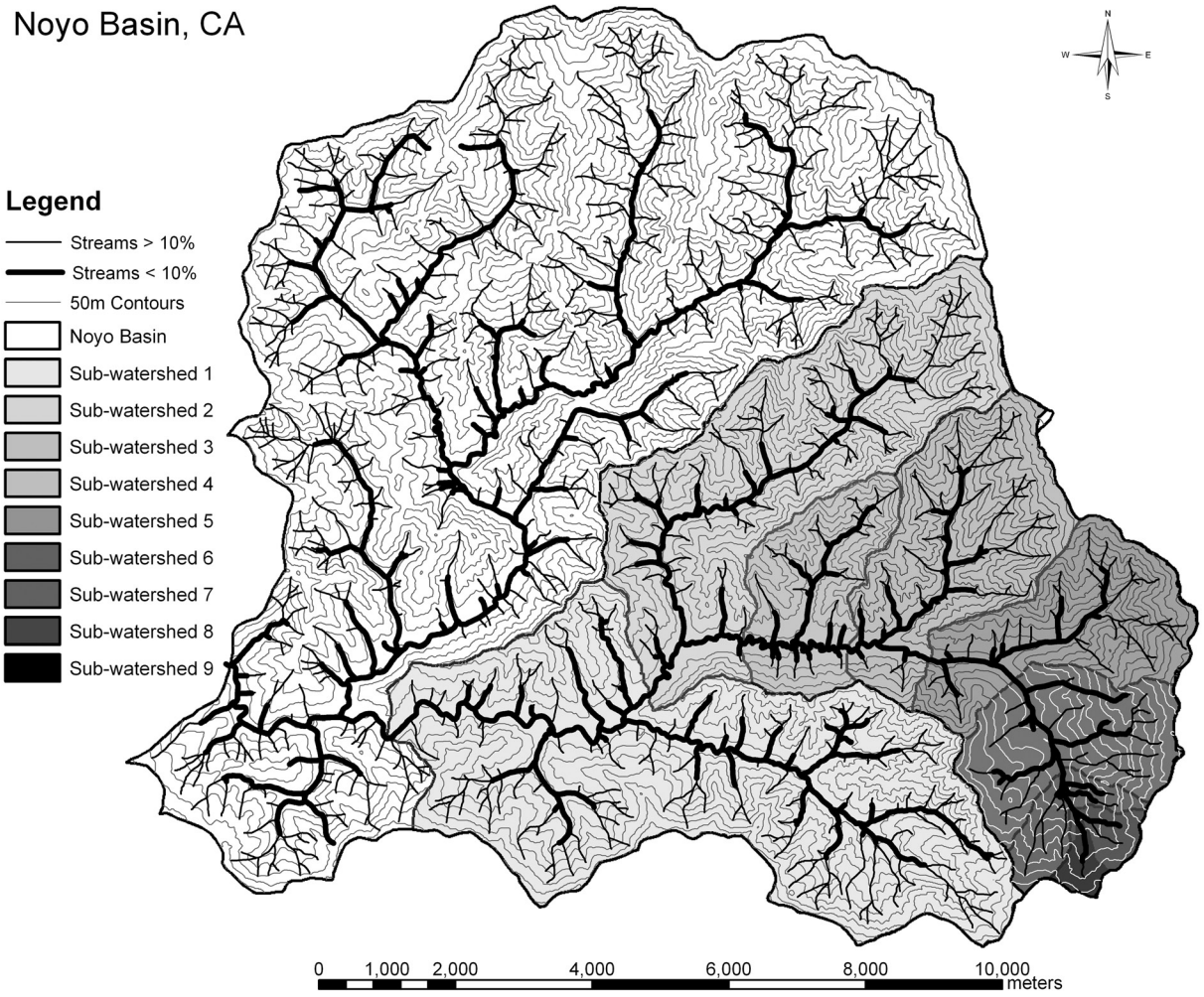

Figure 1. Map of the Upper Noyo River Basin, Mendocino County, northern California. Outlet located at 39°26′N, 123°45′W.

time along channels. These sediment pulses are swept by runoff events, sorted hydraulically, and their particles are broken and abraded during transport. Along any channel path, tributaries introduce local infusions of sediment that mix with channels from other sources [e.g., *Rice and Church*, 1998; *Jacobson and Gran*, 1999]. Might the channel network structure and the dynamic, unsorted additions of sediment lead to scale-invariant patterns of bed load sediment grain size and flux along the channel?

[3] If we look at this from the perspective of examining gravel at a specific location on the riverbed, other questions emerge. Each particle on a gravel bed of a river has a distinct travel history from its source. Some originate at the farthest portions of the contributing watershed, and others only a short distance from a point of observation. Most of the grains are not the size they were when they entered the stream. Commonly, particles entering a stream are derived from the chemical, biotic and mechanical breakdown of bedrock, and this derivation not only imparts a size distribution to the incoming sediment, it also weakens the particles such that subsequent bed load transport downstream causes wear and fragmentation, sometimes quite rapidly. Even relatively unweathered bedrock fragments will be pounded and reduced in size. These downstream fining particles follow the channel network and merge with particles arriving through different channel branches and other parts of the landscape. These branches may access steeper slopes shedding coarser sediment of the same bedrock, or cut into harder bedrock with more durable particles [e.g., *Pizzuto*, 1995]. Does this mingling of sediment with different transport paths and different bedrock sources create a distinct size distribution of bed sediment? Is there a signature of the channel network structure and its bedrock heterogeneity in the size distribution of the sediment?

[4] This seems a reasonable hypothesis in that the channel network structure imposes a travel distribution function to any point along the channel. For example, in Figure 1 the channel network of a catchment is shown, and the corresponding width function is plotted in Figure 2a. The width function gives the number of channel segments along the channel network at a specified distance from the mouth [e.g., *Rodriguez-Iturbe and Rinaldo*, 1997]. Along each interval of distance from the mouth, there is a contributing drainage area, which sets the scale for the amount of sediment entering the channel. For example, in Figures 2b and 2c, the cumulative drainage area and incremental area per unit length entering each channel segment are plotted as

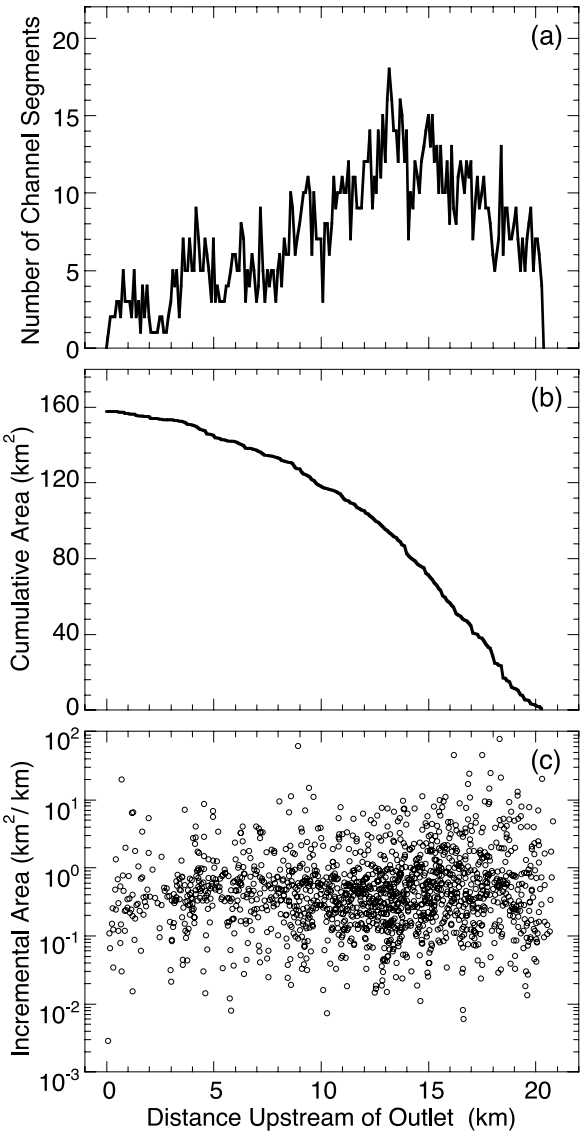

Figure 2. Noyo River channel network characteristics: (a) Width function (distribution of channel segments at specified distance from downstream outlet), (b) cumulative area function, and (c) incremental drainage area per channel segment length.

a function of distance from the mouth. The sum over all upstream distances of the product of the local erosion rate times the local contributing area and the total number of points at that distance from the mouth (i.e., the width function, Figure 2a), gives the total influx of sediment to the channel at the specified distance. If particle breakdown depends on travel distance, then one would expect bigger particles to be derived locally, and finer particles from farther away, and depending on how tributaries come in, the grain size distribution may be tipped toward the coarse or fine fraction.

[5] Watersheds rarely drain homogeneous bedrock, and probably rarely receive grain size distributions that are identical throughout the basin even if the bedrock is relatively uniform. At present, there are essentially no data or theory to tell us what the distribution function of grain sizes entering a channel network is or how that should vary throughout a watershed. Some have argued that fragmentation of bedrock should produce fractal scaling of particle numbers with grain size [e.g., *Turcotte*, 1997; *Perfect*, 1997] and there have been studies of the finer fraction of some soils that suggest multifractal scaling of grain sizes [e.g., *Bittelli et al.*, 1999]. Whether fractal or not, certainly soils, screes and glacial deposits have a wide range of particle sizes [e.g., *Matsuoka and Sakai*, 1999; *Posadas et al.*, 2001; *Hooke and Iverson*, 1995].

[6] A common observation is that the gravel clasts making up the beds of rivers are typically derived from the harder bedrock lithologies underlying the watershed, even when the harder rock types compose a relatively small proportion of the landscape [e.g., *Hack*, 1957; *Brush*, 1961; *Dietrich and Dunne*, 1978; *Parker*, 1991b; *Pizzuto*, 1995]. The network travel distribution function (the width function) operates, then, on materials with differing resistance to breakdown and differing starting grain size distributions which may occur systematically in parts of the basin, or scattered throughout. The network structure leads to injections of sediment into main stem reaches from tributaries of widely differing sizes (Figure 2c) that may deliver sediment of greatly differing durability. Under what conditions do these injections perturb the sediment mass and size distribution of the bed of the main stem [e.g., *Rice and Church*, 1998; *Rice*, 1998] and propagate downstream?

[7] Studies of changes in gravel bed size distributions along channels have focused on the tendency for downstream fining [e.g., *Knighton*, 1980, *Rice and Church*, 1998; *Heller et al.*, 2001; *Gomez et al.*, 2001; *Surian*, 2002; *Moussavi-Harami et al.*, 2004, *Malarz*, 2005]. Field measurements of median grain sizes of the bed surface are typically plotted as a function of distance along a longitudinal profile, and downstream decreases are attributed to either selective sorting or particle size reduction due to abrasion or some combination of these processes. In cases of net deposition along the channel, selective sorting has been shown to be an effective agent of downstream fining [e.g., *Paola et al.*, 1992; *Ferguson et al.*, 1996; *Gomez et al.*, 2001]. Where no net deposition occurs (in rivers actively cutting through bedrock for example) abrasion is held responsible for downstream fining [e.g., *Kodama*, 1994a]. Abrasion of particles appears to follow Sternberg's law

$$D = D_0 e^{-\alpha x} \tag{1}$$

where the initial grain size D_0 wears down to D at distance x from the origin at a rate given by α (1/m) (see reviews by *Parker* [1991a], *Kodama* [1994a, 1994b], *Gomez et al.* [2001], *Lewin and Brewer* [2002], and *Malarz* [2005]). Particles are presumed to wear by shedding silt and clay size mass, rather than by splitting, although splitting could be important in some rock types [*Kodama*, 1994b]. Tumbling experiments support the form of equation (1) and α has been experimentally estimated [e.g., *Kuenen*, 1956; *Adams*, 1978; *Kodama*, 1994b; *Lewin and Brewer*, 2002]. Translation of tumbling experiments to the field setting can be controversial because of the large differences in particle collision dynamics and the absence of weathering in tumbling mills. Alternatively, plots of median or maximum

grain size against distance downstream have been used to parameterize α and D_0 [e.g., *Moussavi-Harami et al.*, 2004; *Malarz*, 2005], but interpretation of such plots requires demonstrating that net storage of sediment is not occurring.

[8] It is reasonable to propose that over a sufficiently long timescale, in upland catchments with active channel incision into bedrock, there is no net storage of sediment in the channel. All sediment entering the channel is either flushed through the system as wash and suspended bed material load, or travels as bed load and abrades to finer particles. The long-term average bed load size distribution at any point on the reach will represent some balance of sediment introduction and abrasion, and it is the size distribution of this load we wish to relate to the channel network and travel paths. For any reach of river the best short-term estimate of that size distribution is probably the spatially averaged subsurface grain size [e.g., *Parker and Klingeman*, 1982; *Parker*, 1990], rather than the size found just at the surface, which is influenced by vertical sorting.

[9] To address the questions posed here, we theoretically derive the effects of grain size input functions and abrasion rates on downstream changes in grain size for simple single-channel basins and for basins with branching networks. As described above, the grain size distribution modeled is the long-term bed load size that passes through a particular reach, not necessarily the surface grain size found on bars. We discover that the abrasion coefficient α sets fundamental length scales in the system beyond which, surprisingly, grain size distributions and total bed load flux become independent of travel distance. Bed load flux becomes independent of drainage basin size, and proportional to the ratio of hillslope erosion rate per unit channel length divided by the abrasion coefficient, α. Furthermore, the theory predicts that if the size distribution of input sediment is relatively broad, abrasion has very little effect on the size distribution of resulting bed load flux. The only way significant downstream fining occurs in this case is if the size distribution of the sediment supplied by the hillslopes decreases downstream. The channel network structure introduces perturbations in bed load flux along the main stem of a watershed, but only influences the size distribution if the tributaries introduce coarser sediment (derived from coarser sediment inputs). Depending on the durability of this coarser sediment, the effect may quickly damp out downstream. Hence, in a watershed with uniform bedrock and small spatial variation in grain size sediment input, abrasion causes little change in bed load grain sizes and instead the size closely reflects the input size distribution. Our findings highlight the need for theory and observations on the grain size distribution of sediment shed to channels.

2. Theoretical Framework

2.1. Assumptions

[10] We make several key assumptions in developing the theory presented below. First, we assume that all sediment delivered by hillslopes to the channel network is either actively transported downstream and out of the watershed as bed load or as suspended load, or, in the case of very large, essentially immobile boulders, are abraded and weathered in place. Hence there is no net deposition of sediment. This is consistent with a tectonically active landscape, where channels and valley floors have only a thin veneer of sediment over bedrock, and is consistent with a relatively long timescale of analysis that averages over shorter-term fluctuations in sediment supply and sediment transport capacity which produce episodes of sediment accumulation in storage reservoirs such as fans and floodplains. As discussed in more detail below, the assumption of no net deposition implies no net selective transport of finer grain sizes because coarse grains would otherwise continuously accumulate over time. Another corollary of the assumption of no net deposition is the assumption that all segments of the channel network receive lateral inputs of sediment from adjacent hillslopes, without interception by intervening storage elements such as floodplains, and that bed load sediment transport is continuous across all tributary junctions.

[11] A second key set of assumptions concerns the simple Sternberg exponential model for particle size reduction with downstream transport (equation (1)). We assume that the Sternberg relation is valid not just for the bulk bed load mass but for individual sediment particles as well, and that the abrasion efficiency parameter α depends only on lithology and is independent of local transport conditions and constant for all grain sizes. There are potentially important physical mechanisms that are thus either lumped into the single model parameter α or are neglected entirely, including abrasion in place of bed surface grains [e.g., *Schumm and Stevens*, 1973], weathering rind formation during floodplain storage [e.g., *Heller et al.*, 2001], rapid initial wear of freshly input hillslope sediments [e.g., *Adams*, 1979] and particle splitting, which may be important in particular lithologies [e.g., *Kodama*, 1994a, 1994b].

[12] Another important assumption is that there is a minimum grain size $D_{\min}$ below which particles travel in suspension and do not contribute to the bed load mass flux or bed load grain size distribution. In all calculations reported here we set $D_{\min} = 2$ mm. We treat the transition from bed load to suspended transport as abrupt, and assume that once in suspension, fine-grained sediments are rapidly transported downstream and out of the watershed. We thus ignore abrasion during suspended transport and the potential contribution of sand to the bed load grain size and mass flux [e.g., *Wilcock et al.*, 2001]. Finally, we assume that sediment production by channel incision into bedrock can be ignored because it makes a negligible contribution to the total bed load supply.

2.2. Analytical Development

[13] In this section, we derive the probability distribution (pdf) of bed load grain diameter D, in terms of both size and mass, given the probability distribution of the entering sediment diameter D_e and the spatially variable load of sediment $q(L)$ to the river. We start with the simplest case of constant (uniform) size of entering sediment and a spatially uniform lateral load and progress to the most complex case of spatially variable probability distribution of entering sediment and spatially variable lateral load.

2.2.1. Uniform Load $q(L) = q$, Constant D_e

[14] The lateral uniform load (mass per unit stream length per unit time) is $q = N_e k D_e^3$ where N_e is the number of grains

entering the stream, D_e is the constant size of the grains and $k = \rho_s\pi/6$ where ρ_s is the density of the sediment. Following Sternberg's law $D(L) = D_e \cdot e^{-\alpha L}$, a grain of initial diameter D_e will reach a diameter $D_{\min}$ and go to suspension after a distance L_D^* given by

$$L_D^* = \frac{1}{\alpha} \cdot \ln\left(\frac{D_e}{D_{\min}}\right) \tag{2}$$

For any distance $L \geq L_D^*$ along the river, the bed load grain size distribution will be at steady state and will be independent of L, while for all distances $L < L_D^*$ a dependence on distance L is expected. It can be shown (see Appendix A) that for a uniform unit load of q, the pdfs of the bed load sediment diameter by grain $f_b^g(D)$ and by mass $f_b^m(D)$ take the following forms. For $L \geq L_D^*$ and $D_{\min} \leq D \leq D_e$

$$f_b^g(D) = \frac{1}{\alpha L_D^* D} = \frac{1}{D} \cdot \frac{1}{\ln\left(\frac{D_e}{D_{\min}}\right)} \tag{3}$$

$$f_b^m(D) = \frac{3}{D_e^3 - D_{\min}^3} \cdot D^2 \tag{4}$$

and for $L < L_D^*$ and $D_e e^{-\alpha L} \leq D \leq D_e$

$$f_b^g(D) = \frac{1}{\alpha L D} \tag{5}$$

$$f_b^m(D) = \frac{3}{D_e^3(1 - e^{-3\alpha L})} \cdot D^2 \tag{6}$$

For values of D outside the specified intervals, the pdfs are zero. The mass flux of bed load sediment M at distance L downstream can be shown to be (see Appendix B), for $L < L_D^*$

$$M(L) = \frac{q}{3\alpha}\left(1 - e^{-3\alpha L}\right) \tag{7}$$

and $L \geq L_D^*$

$$M(L) = M_{ss} = \frac{q}{3\alpha}\left[1 - \left(\frac{D_{\min}}{D_e}\right)^3\right] \tag{8}$$

where M_{ss} stands for the steady state mass flux, and L_D^* is given by equation (2).

[15] Importantly, this means that beyond the distance L_D^* the bed load flux is constant and no longer increases with drainage area, as discussed at length in section 3 below. Note that 95% of the mass flux is achieved at the distance $L_{M,0.95}^*$ at which

$$1 - \exp\left[-3\alpha L_{M,0.95}^*\right] = 0.95 \tag{9}$$

which results in

$$L_{M,0.95}^* \cong 1/\alpha \tag{10}$$

An example illustrating these theoretical results is presented below in section 2.3.

2.2.2. Uniform Load $q(L) = q$, pdf of Entering Sediment $f_e^g(D_e)$

[16] Let the entering sediment have a probability distribution by grain, and correspondingly by mass, denoted by $f_e^g(D_e)$, and $f_e^m(D_e)$ respectively. First, we note that $f_e^g(D_e)$ and $f_e^m(D_e)$ relate to each other. One might specify $f_e^g(D_e)$ as lognormal, and derive the pdf of $f_e^m(D_e)$ by acknowledging that mass $= k \cdot D_e^3$, where $k = \pi \cdot \frac{\rho_s}{6}$. We can write that

$$f_e^m(D_e) = \frac{D_e^3 \cdot f_e^g(D_e)}{\int_{D_{\min}}^{\infty} D_e^3 \cdot f_e^g(D_e) dD_e} \tag{11}$$

i.e., the pdf by number of grains is multiplied by the mass of the grain and normalized by the total mass to render it a pdf by mass.

[17] Having an unbounded probability distribution of grain sizes implies that very large particles (theoretically of infinite size) are possible albeit with a very small probability. Thus defining a length L_D^* at which a steady state by grain size is reached is not as straightforward as when the entering sediment is of constant size. In this case, an upper maximum size $D_{\max}$ must be externally imposed based on either deterministic or probabilistic reasoning. In the deterministic case, the value of $D_{\max}$ may be prespecified based on physical considerations, e.g., rare particles larger than $D_{\max}$ are too large to be transported with the flow and do not contribute to the bed load. This $D_{\max}$ value implies a probability of nonexceedance $p = F_e^m(D_{\max})$, where $F_e^m(D_e)$ is the cumulative probability by mass, at which the pdf of the entering sediment will have to be truncated. In the probabilistic case, a probability of nonexceedance p may be prespecified (say, 95%) and the corresponding value of $D_{\max,p}$ (quantile) can be computed as $D_{\max,p} \equiv F_e^{m^{-1}}(p)$. In both cases, the truncated pdf (below by $D_{\min}$ and above by $D_{\max,p}$) of the entering sediment has to be used in the calculations. On the basis of this size $D_{\max,p}$ an equivalent distance $L_{D,p}^*$ to steady state bed load pdf by mass can be defined as

$$L_{D,p}^* = \frac{1}{\alpha} \cdot \ln\left(\frac{D_{\max,p}}{D_{\min}}\right) \tag{12}$$

It can be shown that the bed load sediment pdfs are given as for $L \geq L_{D,p}^*$ and $D_{\min} \leq D \leq D_{\max,p}$

$$f_b^g(D) = \frac{1}{D} \cdot \frac{\int_D^{D_{\max,p}} f_e^g(D_e) dD_e}{\int_{D_{\min}}^{D_{\max,p}} f_e^g(D_e) \ln\left(\frac{D_e}{D_{\min}}\right) dD_e} \tag{13}$$

and for $L < L_{D,p}^*$ and $D_{\min} \leq D \leq D_{\max,p}$

$$f_b^g(D) = \frac{1}{D} \cdot \int_{\min(D, D_{\max}(L))}^{\max(D_{\max}(L), e^{\alpha L} D)} f_e^g(D_e) dD_e / K \tag{14}$$

where

$$K = \int_{D_{\min}}^{D_{\max(L)}} f_e^g(D_e) \ln\left(\frac{D_e}{D_{\min}}\right) dD_e + \alpha L \int_{D_{\max(L)}}^{D_{\max,p}} f_e^g(D_e) dD_e$$

$$D_{\max(L)} \equiv D_{\min} \cdot e^{\alpha L}$$

[18] From the pdf of the bed load sediment by grain, one can derive the pdf of the bed load sediment by mass using equation (11) so these equations are not displayed here. Finally, the mass flux of bed load sediment as a function of distance downstream can now be derived. This involves a trivial extension of equations (7) and (8), i.e., for $L < L^*_{D,p}$

$$M(L) = \frac{q}{3\alpha}\left(1 - e^{-3\alpha L}\right) \tag{15}$$

where now

$$q = N_e k \int_{D_{\min}}^{D_{\max,p}} D_e^3 f_e^g(D_e) dD_e$$

and for $L \geq L^*_{D,p}$ the steady state mass flux becomes

$$M_{ss} = \frac{q}{3\alpha} \cdot \left[1 - D_{\min}^3 \Big/ \int_{D_{\min}}^{D\max,p} D_e^3 f_e^g(D_e) dD_e\right] \tag{16}$$

Because the second term in brackets will generally be very small, the steady state mass flux M_{ss} can be approximated as $q/3\alpha$, providing a simple estimate for long-term bed load downstream of $L^*_{D,p}$. Assuming a lognormal pdf of the entering sediment by number of grains (which we will use in the example applications below), it can be shown that the steady state mass becomes

$$M_{ss} = \frac{N_e k}{3\alpha} \cdot \exp\left[3\mu_{\ln D_e} + \frac{9}{2}\sigma^2_{\ln D_e}\right] \tag{17}$$

where $\mu_{\ln D_e}$ and $\sigma_{\ln D_e}$ are the mean and standard deviation of the lognormal distribution. We note that, as before, 95% of the steady state mass is reached at distance $L^*_M = 1/\alpha$ which does not depend on the pdf of the entering sediment but only on the abrasion coefficient. An example illustrating these theoretical results is presented in section 2.3.

2.2.3. Nonuniform Load $q(L)$, D_e = Constant

[19] In the previous two cases, we treated the lateral load of entering sediment per unit stream length per unit time as uniform. Now, we consider the case of a spatially variable load, i.e., load that depends on the distance L downstream. Such a case is motivated by the need to consider spatial variations in hillslope sediment supply due to differing erosion rates, or variations in the fraction of the sediment supply in the bed load size range due to differences in hillslope soil or bedrock properties.

[20] Let $q(L)$ denote the load rate per unit stream length and unit time as a function of distance L. It can be shown that the bed load sediment pdf by grain is given, for $L \geq L^*_D$ and $D_{\min} \leq D \leq D_e$, by

$$f_b^g(D) = \frac{1}{\alpha D} \cdot \frac{q\left(L - \frac{1}{\alpha} \cdot \ln\left(\frac{D_e}{D}\right)\right)}{\int_{L-L^*_D}^{L} q(x)dx} \tag{18}$$

and for $L < L^*_D$ and $D_e e^{-\alpha L} \leq D \leq D_e$

$$f_b^g(D) = \frac{1}{\alpha D} \cdot \frac{q\left(L - \frac{1}{\alpha} \cdot \ln\left(\frac{D_e}{D}\right)\right)}{\int_{0}^{L} q(x)dx} \tag{19}$$

The pdfs by mass can be easily derived from the above pdfs and equation (11). An example illustrating the above result is presented in section 3.3 where the load function $q(L)$ is patterned after the width function of a river network.

2.2.4. Nonuniform Load $q(L)$, pdf of Entering Sediment $f_e^g(D_e)$

[21] In a similar manner as before, we can derive the following expression for the bed load pdf by grain size for $L \geq L^*_{D,p}$ and $D_{\min} \leq D \leq D_{\max,p}$

$$f_b^g(D) = \frac{1}{\alpha D} \cdot \int_D^{D_{\max,p}} q\left(L - \frac{1}{\alpha} \cdot \ln\left(\frac{D_e}{D}\right)\right) f_e^g(D_e) dD_e / K \tag{20}$$

where

$$K = \int_{D_{\min}}^{D_{\max,p}} f_e^g(D_e) \left(\int_{L - \frac{1}{\alpha}\ln\left(\frac{D_e}{D}\right)}^{L} q(x)dx \right) dD_e$$

For $L < L^*_{D,p}$ the equation becomes too complex to display here.

2.2.5. Nonuniform Load $q(L)$, pdf of D_e Varying Downstream

[22] This is the most general case and allows for the parameters of the pdf of the entering sediment to depend on the distance downstream. This might occur when hillslope sediment supply changes systematically downstream or tributaries enter the main stem and contribute sediment with distinct grain size distributions reflecting differing upstream lithologies, hillslope processes or erosion rates. The equations become cumbersome to write but not conceptually difficult to extend from those of the previous cases.

2.3. Application to a River Reach

[23] We illustrate the above theoretical results with an example application that considers a river reach having a uniform lateral load rate of entering sediment. We set $D_{\min}$ = 2 mm, and the abrasion coefficient $\alpha = 0.0002$ m^{-1}. In the first case we consider a constant entering size D_e = 500 mm. Note that for this case, the distance L^*_D required to wear the sediment down to the suspension size and the distance at which steady state mass flux (at the 95% level) is achieved are L^*_D = 27.6 km and $L^*_M \simeq 5$ km (computed by equations (2) and (10), respectively).

[24] Figure 3a shows the pdf of bed load sediment by grain f_b^g(ln D) for various distances L downstream with a

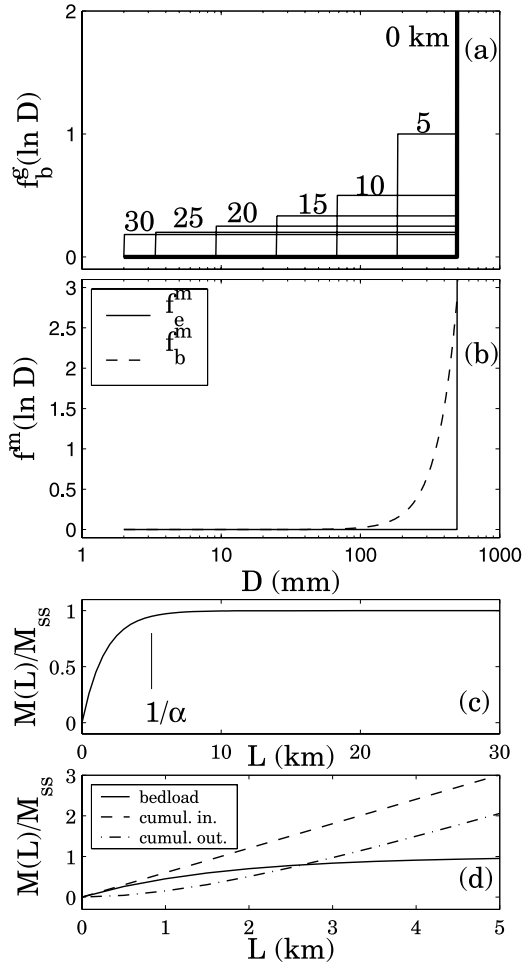

Figure 3. Entering sediment of constant grain size (D_e = 500 mm) and constant lateral load rate: (a) evolution of the pdf of bed load grain diameter, with frequency in terms of number of grains, for 5 km increments of downstream distance L. Note the steady state pdf (for L = 30 km) with an equal number of grains in each size (above $D_{\min}$ = 2 mm). (b) Steady state pdf of bed load grain diameter, with frequency in terms of mass, achieved at distance $L_D^* \simeq 27.6$ km. (c) Bed load mass flux as a function of distance downstream, normalized by the steady state mass flux M_{ss}. (d) Normalized bed load sediment flux, cumulative input flux to the bed load from entering sediment, and cumulative output flux from bed load to suspended load, as a function of downstream distance (note that only the first 5 km are displayed before steady state is reached).

constant size of entering sediments D_e = 500 mm (from L = 0 km to L = 30 > 27.6 km at which the steady state pdf is achieved). Note that since the pdf of D is $\frac{1}{\alpha L_D^* D}$ (equation 5), the pdf of ln D which is given by

$$f(\ln D) = D \cdot f(D) \tag{21}$$

becomes a uniform pdf equal to $1/\alpha L$. The area under each pdf in Figure 3a is equal to 1 as the range of D over which each pdf is defined is αL. For example, for L = 10 km, αL = 2.0, and the corresponding value on the probability axis is 0.5, such that the area under the pdf is 1.0.

[25] Figure 3b shows the pdf by mass of the entering and bed load sediment. Note that in Figure 3b we again plot the pdf of ln D (i.e., f_b^m (ln D) versus ln D) because a lognormal pdf in D_e (which will be considered in the next section) would plot as Gaussian or normal curve. Using the transformation of equation 11, the pdf by mass, which goes as $1/D^2$, becomes a pdf that decays as $1/D$, as displayed in Figure 3b.

[26] Figure 3c shows the mass flux as a function of distance L downstream $M(L)$, normalized by the steady state mass flux M_{ss}, and illustrates how $M(L)$ reaches approximate steady state at $L = 1/\alpha$. Figure 3d shows the normalized mass flux as a function of downstream distance together with the cumulative sediment flux input and output, focusing in the upstream 5 km of the river reach. As the bed load flux $M(L)$ approaches steady state, the rate of suspended load (silt and sand) production begins to match the rate of sediment input; the difference between the cumulative input and output curves is a constant equal to the bed load flux. Figure 4 shows the mass flux as a function of distance downstream for different values of the abrasion coefficient α and illustrates how rock durability, as parameterized by α, controls the magnitude of steady state bed load flux and the distance required to reach steady state (equations (7) and (10)). For Figure 4 we used an erosion rate E of 0.1 mm/year, a contributing area per unit length a of 0.5 km^2/km and a density of the entering sediment of ρ_s = 2500 kg/m^3 and computed the load rate $q = E\ a\ \rho_s$.

[27] We now consider a second example application to contrast the cases of constant grain size of entering sediment as analyzed above with the case of a probability distribution of entering sediment which can be narrow (sorted sediment) or wide (unsorted sediment). The practical use of this example will be to quantitatively assess the effect of the pdf of the sediment entering from the hillslopes to the bed load grain size distribution found downstream. We assume a

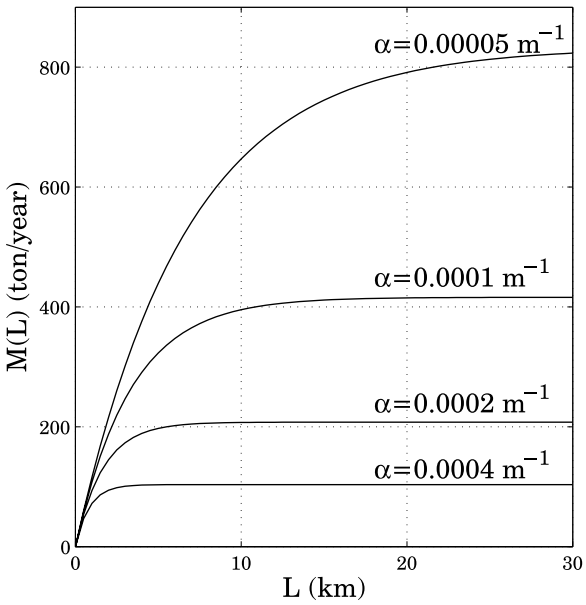

Figure 4. Mass flux $M(L)$ as a function of distance downstream L for different values of the abrasion coefficient α. See text for explanation of the other parameters used for this computation.

Table 1. Comparison of the Statistical Moments of the Entering and Bed Load Grain Size Distributions for Constant Size and Three Lognormal pdfs of Entering Sediment by Mass[a]

pdf	Constant Size	LN1	LN2	LN3
$\mu_e^m = \mu_{\ln D}^m$	6.21	5.34	4.46	3.20
$\mu_b^m = \mu_{\ln D}^m$	5.88	5.01	4.14	3.00
$D_{50,e}$	500 mm	211 mm	89 mm	23 mm
$D_{50,\,b}$		150 mm	65 mm	18 mm
$\sigma_e^m = \sigma_{\ln D_e}^m$	0	0.45	0.90	1.39
$\sigma_b^m = \sigma_{\ln D}^m$	3.333	0.56	0.95	1.34
$S_e^m = S_{\ln D_e}^m$	0	−0.34	−0.33	+0.17
$S_b^m = S_{\ln D}^m$	−2.0	−0.59	−0.33	+0.24
$K_e^m = K_{\ln D_e}^m$	0	2.8	2.8	2.1
$K_b^m = K_{\ln D}^m$	9.0	3.6	2.8	2.1

[a]Subscript e indicates entering, and subscript b indicates bed load. Note that for all pdfs the value of $D_{\max}$ = 500 mm (ln 500 = 6.21), which corresponds to the 5% exceedance quantile.

lognormal distribution for the entering sediment by grain. We remind the reader that a lognormal pdf is specified by its two parameters $\mu_{\ln D_e}$ and $\sigma_{\ln D_e}$,

$$f_e^g(D_e) = \frac{1}{\sqrt{2\pi}\sigma_{\ln D_e} \cdot D_e} \cdot \exp\left[-\frac{\left(\ln D_e - \mu_{\ln D_e}\right)^2}{2\sigma_{\ln D_e}^2}\right] \tag{22}$$

and that the statistics of D_e are given as

$$\begin{aligned} \mu_{D_e} &= e^{\mu_{\ln D_e}} + \frac{\sigma_{\ln D_e}^2}{2} \\ \sigma_{D_e} &= \mu_{D_e} \cdot \left(e^{\sigma_{\ln D_e}^2} - 1\right)^{\frac{1}{2}} \end{aligned} \tag{23}$$

where $e^{\mu_{\ln De}}$ is the geometric mean and also the median of D_e. It can be shown that if $f_e^g(D_e)$ is lognormal then $f_e^m(D_e)$ is also lognormal with parameters

$$\begin{aligned} \mu_{\ln D_e}^m &= \mu_{\ln D_e} + 3\sigma_{\ln D_e}^2 \\ \sigma_{\ln D_e}^m &= \sigma_{\ln D_e} \end{aligned} .$$

It follows that the D_{50} by mass parameter typically reported relates to the parameters of the grain size distribution of the entering sediment by

$$D_{50} = \exp\left(\mu_{\ln D_e} + 3\sigma_{\ln De}^2\right).$$

[28] There are several ways by which one can specify the lognormal distribution parameters such that the results can be contrasted with those obtained for the constant size D_e of entering sediment presented in the previous section. A simple way to specify the lognormal pdf of the entering sediment would be to set $\mu_{\ln D_e}$ = ln 500 which would imply a geometric mean of grain size equal to 500 mm, which was the constant $D_e = D_{\max}$ value used in the previous example. The variance $\sigma_{\ln D_e}$ could be changed to mimic a narrow or wide pdf of grain size. Such a specification would result in 95% quantiles which would vary widely and would be hard to compare the results to those obtained using the maximum size $D_{\max}$ = 500 mm of the previous case. Since the maximum size of D_e sets the "length scale" of the system, in terms of the distance downstream at which steady state pdf of bed load sediment is achieved, we propose that a more meaningful comparison would result if the lognormal pdfs were specified such that the corresponding systems have comparable length scales to each other and to the system of constant grain size. Thus we consider lognormal pdfs such that their upper 5% quantile is reached at $D_{\max}$ = 500 mm and by specifying $\sigma_{\ln D_e}^m$ = 0.1, 0.5, and 1.0 we derive the corresponding values of $\mu_{\ln D_e}$. The parameters of the lognormal pdfs are given in Table 1 and the pdfs are displayed in Figure 5.

[29] For the three different lognormal pdfs of entering sediment by mass, we compute the steady state bed load pdfs by mass and these are shown in Figure 6. As the distribution of the entering sediment widens (less sorted sediment entering from the hillslopes), the steady state pdf of the bed load approaches a shape that is close to the shape of the pdf of the entering sediment and is not very sensitive to further changes in the variance of the entering sediment pdf. To quantify this further, we have computed (via numerical evaluation) the moments of the derived pdfs (i.e., mean $\mu_b^m \equiv \mu_{b,\ln D}^m$, standard deviation $\sigma_b^m \equiv \sigma_{b,\ln D}^m$, coefficient of skewness $S_b^m \equiv S_{b,\ln D}^m$ and coefficient of kurtosis $K_b^m \equiv K_{b,\ln D}^m$). These are shown in Table 1 together with the same parameters of the entering sediment pdfs by mass. Note that the reported μ_e^m and σ_e^m are not exactly the specified parameters of the entering sediment LN pdf but rather the numerically computed moments of the resulting truncated pdfs. For example, for LN1 the specified parameter $\sigma_{\ln D_e}^m$ was 0.1 but the computed standard deviation $\sigma_e^m = \sigma_{\ln D_e}^m$ shown in Table 1 was 0.09. Figure 7 shows the ratio of the means of the entering to bed load sediment, the ratio of the standard deviations and coefficients of skewness and kurtosis of the bed load sediment pdf by mass, all for ln D. We observe that as the variance of the entering sediment pdf increases the coefficient of skewness of the bed load sediment approaches zero and the coefficient of kurtosis approaches 3, implying an approach to a normal distribution for ln D, or lognormal

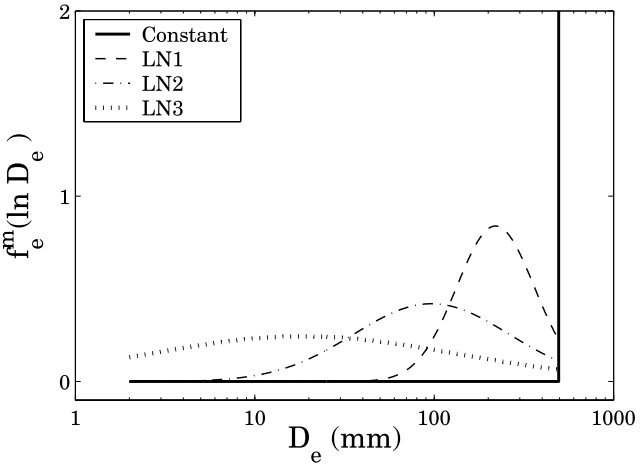

Figure 5. Specification of three lognormal pdfs of entering sediment by mass such that for all pdfs the probability of exceeding D_e = 500 mm is 5%. The parameters of the lognormal pdfs are shown in Table 1 (see text for explanation).

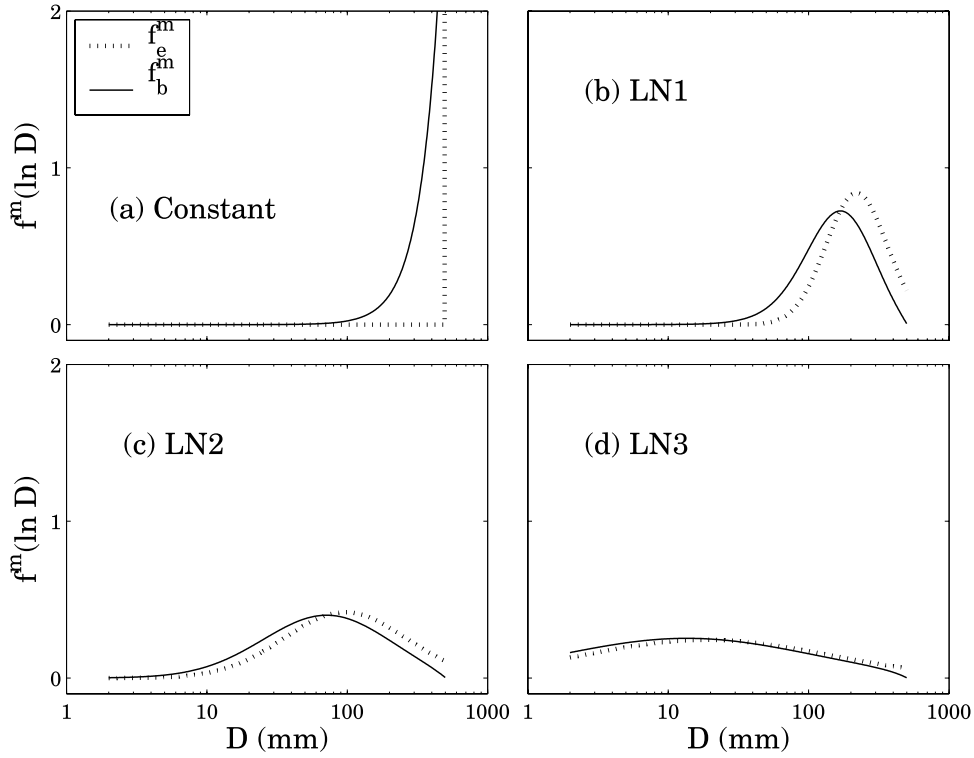

Figure 6. Comparison of pdfs of entering sediment by mass $f_e^m(\ln D_e)$ (dashed lines) to those of the steady state pdfs by mass of the bed load f_b^m (ln D) (solid lines) for (a) the constant size D_e and (b–d) the three pdfs of Table 1 (narrow to very wide).

distribution for the bed load sediment. We conclude that the wider the pdf of the entering sediment, the closer the bed load sediment pdf by mass is to that of the entering sediment. Although little is known about the pdfs of sediments delivered to channels by hillslopes, it is reasonable to assume that the most common case is a very wide (unsorted) distribution.

3. Application to Channel Networks

[30] Several important and previously unrecognized insights emerge from the theoretical results of the preceding section. First, for the case of input sediment grain size distributions that are spatially uniform and poorly sorted, the effect of abrasion during downstream transport on the bed material grain size distribution may be so small as to be undetectable in the field. Because of continuous downstream resupply of the input size distribution, the bed material should essentially mirror what the channel is receiving from adjacent hillslopes. This implies that, in the absence of net deposition due to selective transport, measurable spatial variations in bed material size distributions result primarily from spatial variations in the size of sediments entering the channel network.

[31] A second key result that emerges from the theory is that the downstream trend in the long-term average bed load flux does not scale in a simple way with the upstream contributing drainage area. Rather, the bed load mass grows only until the rate of silt production by abrasion matches the rate of coarse sediment input, at which point the bed load flux becomes constant and independent of drainage area. Importantly, for a given abrasion rate coefficient (α), the steady state bed load mass is achieved relatively rapidly (equation (10)), compared to the distance required for the bed material grain size distribution to reach steady state (equation (2)). As illustrated in detail below, this implies that spatial variations in bed load flux created by the branching structure of drainage networks will not depend simply on the pattern of accumulation of drainage area at tributary junctions, but will depend instead on the upstream travel distances of discrete sediment travel pathways, relative to the distances at which mass L_M^* and sediment grain size L_D^* reach steady state.

[32] In this section we use the theory to investigate the potential sources of variation in bed material grain size distributions through channel networks. To simulate spatial variation in input sediment sizes and rates of abrasion, we focus on the effect of lithologic heterogeneity, assuming that rock properties will strongly influence the size distribution of hillslope sediments and the rate of particle breakdown in the channel. Although the size of input sediments should also depend on the rates and styles of hillslope sediment production and transport, for simplicity we assume a spatially uniform landscape erosion rate in all of the following calculations. Thus the sediment loading rate $q(L)$ can be written as

$$q(L) = \rho_s E\, a(L) \tag{24}$$

where ρ_s is the density of both bedrock and bed load sediment (kg/m^3), E is erosion rate (m/yr), and $a(L)$ is the incremental addition of drainage area per unit channel length (m). Note that $a(L)$ can be spatially variable, reflecting in part the channel network structure.

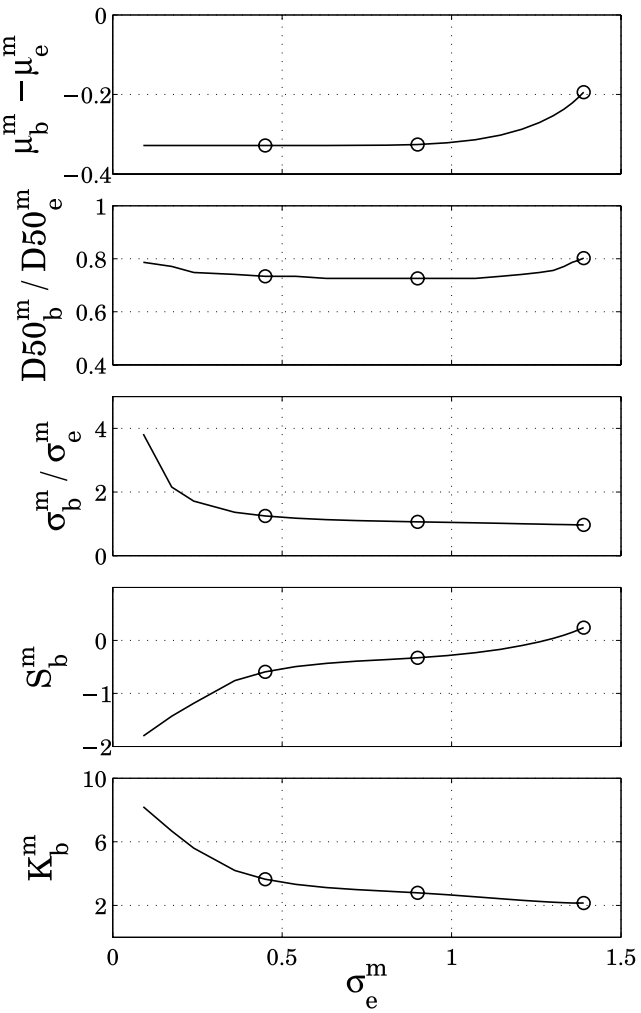

Figure 7. Moments of the bed load pdf as a function of the variance of the entering sediment pdf: (a) difference in mean size of entering μ_e^m and bed load μ_b^m sediment, (b) ratio of geometric mean diameter of bed load to entering sediment, (c) ratio of standard deviations of bed load and entering sediment σ_b^m/σ_e^m, (d) coefficient of skewness of bed load sediment, and (e) coefficient of kurtosis of bed load sediment. Circles indicate values for the three lognormal distributions, LN1, LN2, and LN3, of Figures 5 and 6 and Table 1.

[33] A simple example application of the theory relates to the common observation that river bed sediments are often enriched in the more durable lithologies that outcrop within the upstream drainage area. For an illustrative case where a single geologic unit is composed of two rock types of differing durability (e.g., interbedded sandstones and mudstones), we can predict the mass fraction in the bed material of the more durable rock type as a function of its mass fraction in the input sediment and the ratio of the abrasion coefficients of the two rock types, as shown in Figure 8. For this calculation we assume that the downstream travel distance L exceeds the length L_M^* required to reach the steady state mass M_{ss}, which is set by the inverse of the abrasion coefficient for the more durable rock (i.e., $1/\alpha_h$). Note that equations (7) or (15) could be used for the slightly more complex case where $L < 1/\alpha_h$.

[34] Figure 8 shows that as the durability of the two rock types diverges, the relative enhancement in the hard rock fraction on the bed is approximately proportional to the ratio of abrasion coefficients (α_w/α_h). As the hard rock becomes the dominant component of the bed material, with larger values of α_w/α_h, the sensitivity of the bed composition to the durability contrast declines. For very large differences in abradability, the hard fraction dominates irrespective of its mass fraction in the hillslope source material. Implicit in this calculation is the assumption that abrasion coefficients for the two rocks are independent. We expect, however, that the abradability of weak rocks should be enhanced by the presence of more durable rocks in the bed load sediment mixture; at present no experimental data are available to constrain this relationship.

[35] In the remainder of this section, we further explore the influence of particle abrasion and travel distance on bed material grain size distributions by considering downstream fining, variations in bed load mass and particle size across tributary junctions, and the effect of differing drainage basin shapes as represented by the width function.

3.1. Downstream Fining

[36] For more than a century, a downstream reduction in bed material grain size has been reported in studies of river networks in a diverse set of landscapes [e.g., *Gilbert*, 1877; *Hack*, 1957; *Brush*, 1961; *Kodama*, 1994a; *Gomez et al.*, 2001]. Recently, debate has centered on the question of whether selective transport or particle abrasion is the dominant control in rates of downstream fining [e.g., *Parker*, 1991a, 1991b; *Kodama*, 1994a, 1994b]. In depositional environments selective transport has been shown to be responsible for very rapid fining over short distances [e.g., *Paola et al.*, 1992; *Ferguson et al.*, 1996]. Many workers have assumed that where selective transport cannot

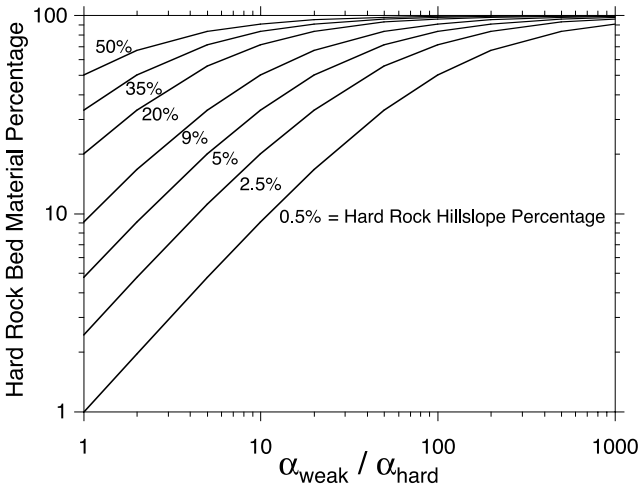

Figure 8. Variation in percentage by mass of hard rock, in a bed load sediment mixture of both weak and hard bedrock source material, as a function of the ratio of abrasion coefficients for the weak and hard rock types (α_w/α_h), for $L > 1/\alpha_h$. Curves shown are for various mass percentages of the hard rock in the coarse sediment entering the channel network.

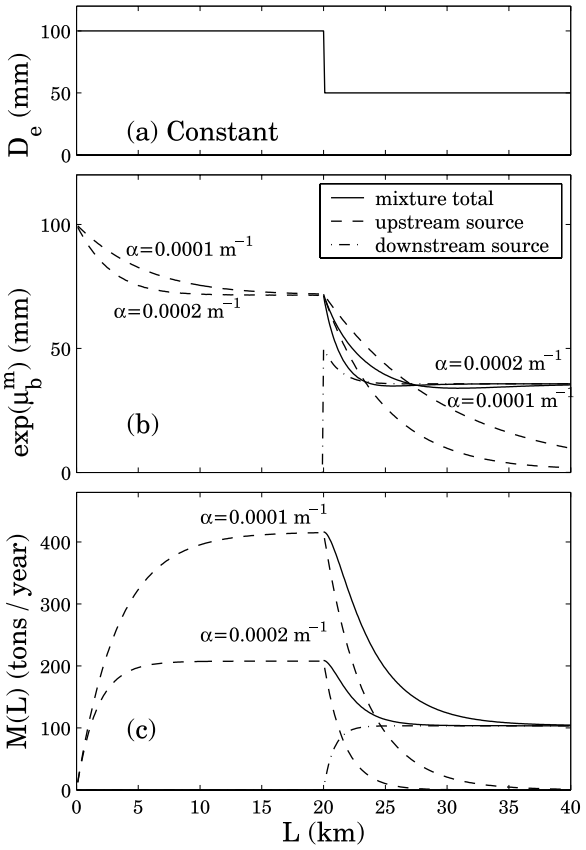

Figure 9. Downstream fining example. Variation with downstream distance L of (a) entering sediment uniform grain size, (b) geometric mean diameter of the bed load, and (c) the bed load mass flux. Results are shown for two different abrasion coefficients (α = 0.0001/m and α = 0.0002/m) for the upstream coarse sediment (D_e = 100 mm); for downstream source sediment (D_e = 50 mm), α = 0.0004/m. Also shown are the grain size and mass flux for the bed load mixture downstream of the lithologic contact at L = 20 km.

fully explain observed fining rates, then abrasion must be responsible for the balance of the size reduction [e.g., *Rice*, 1998; *Gomez et al.*, 2001; *Moussavi-Harami et al.*, 2004]. As shown by the theoretical results presented above in section 2, however, abrasion can only be effective in reducing bed material size when there is a downstream change in the grain size distribution supplied by hillslopes to the channel network.

[37] We can consider two kinds of downstream changes in input grain size distribution, gradual and abrupt. Gradual fining of the coarse sediment supply is probably common in actively incising landscapes for a number of reasons. The highest ridges that make up the watershed divide furthest from the drainage basin outlet are likely to have the steepest average hillslope gradients. To the extent that geologic materials and structure influence channel network architecture, the more distal portions of the watershed are also more likely to be underlain by more durable bedrock. In transient landscapes, where erosion rates are not spatially uniform, it may often be the case that higher erosion rates occur on the steeper slopes in low-order subbasins. In large watersheds, gradients in temperature and precipitation may result in a greater role at higher elevations for mechanical (versus chemical) weathering processes in producing transportable regolith. Each of the these factors may correlate with a coarser hillslope sediment size distribution. Moreover, hillslope sediment production and transport processes likely to supply coarse material to the drainage network, such as debris flow generating landslides, are also more likely to deliver sediment to the steeper channels further from the outlet. Abrupt changes in input grain sizes can occur where channels cross lithologic contacts, and at tributary junctions where channels draining different lithologic units, or landscapes of differing erosional characteristics, combine to form a new bed load mixture.

[38] Here we explore two downstream fining scenarios, each of which is driven by an abrupt change in the grain size distribution of the supplied sediments. We focus on abrupt supply transitions because for the case of a gradual downstream reduction in the input grain size, the change in bed material size distribution should closely track the changing input; bed load fining rate is specified precisely by the input fining rate as long as the characteristic scale over which D_e varies is greater than L_D^*. The close coupling of the bed load and input distributions will also occur when the fining of the supply coincides with a gradual change in mass input rate $q(L)$.

3.1.1. Fining in a Simple Channel

[39] In the first example, we consider a simple main stem channel without major tributary inputs, where the channel receives a spatially uniform rate of sediment mass input (i.e., $q(L)$ is constant). This is perhaps equivalent to a narrow bedrock canyon where sediment is supplied predominantly from the canyon side slopes. As depicted in Figure 9a, we simulate the crossing of a lithologic contact at the midpoint of a 40 km long channel by imposing an abrupt reduction in the input size of a uniform grain size (D_e), from 100 mm to 50 mm. The coarser sediment supplied upstream is also assumed to be more durable than the finer downstream supply, hence it has a lower value of the abrasion coefficient α.

[40] Figure 9b shows the downstream change in the geometric mean of the bed load size distribution, for both the upstream- and downstream-supplied sediments, and for the total bed load mixture below the contact. Upstream of the contact the mean grain size declines initially and then stabilizes, due to the evolution of the bed load pdf away from the entering sediment pdf of a single grain size spike (as in Figure 3b and Table 1). Results for two values of upstream sediment α are shown; the evolution of the bed load distribution is more rapid for the less durable case (α = 0.002/m) than for the case of more durable rock (α = 0.001/m). For both values of upstream α, the bed load pdf reaches steady state before the lithologic contact at L = 20 km. Immediately downstream of the contact the supply shifts to the less durable (α = 0.004/m), finer-grained sediment, and the mean grain size of the bed load mixture (labeled "total") declines rapidly until it stabilizes at a value equal to the mean of the steady state bed load pdf determined by the input size distribution.

[41] The fining downstream of the contact occurs for three reasons. First, abrasion of the coarse material supplied from upstream is no longer balanced by resupply of coarse

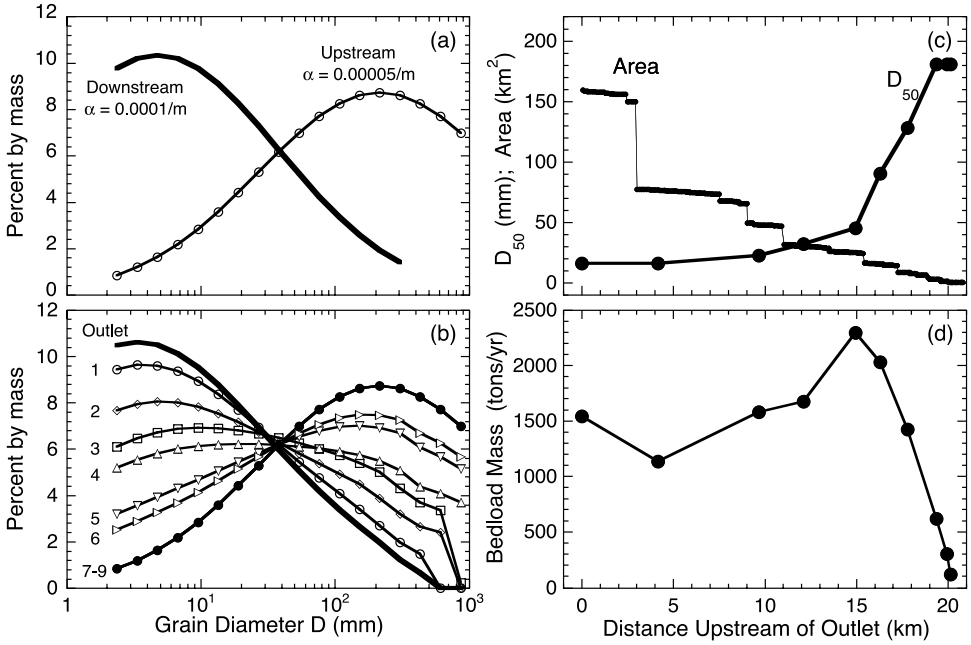

Figure 10. Simulated downstream fining in the Noyo river basin. (a) Entering size distributions for the more durable (α = 0.00005/m) upstream (x > 19 km) sediment and less durable (α = 0.0001/m) downstream sediment. (b) Bed load sediment size distributions for nine nested subbasins and the outlet (locations shown in Figure 1). (c) Variation in median grain size and drainage area with distance upstream of the outlet along the main stem. (d) Predicted annual bed load mass flux with distance upstream of the outlet along the main stem.

material, and the particles of the upstream lithology that cross the contact are progressively reduced in size until all have been converted to silt and sand and swept away in suspension (Figure 9c). Second, the mean size of the newly introduced finer material also declines as its pdf evolves from the initial spike input to the steady state bed load pdf (Figure 3b). Third, the mean of the resulting bed load mixture is an average of the upstream- and downstream-derived materials (both of which are declining), weighted by the relative mass of each component of the mixture. As shown in Figure 9c, the mass of the upstream component of the mixture drops off rapidly below the contact, while the mass of the downstream component climbs to its steady state value. The rate of mass loss of the coarse fraction, and thus the rate of fining of the bed load sediment mixture, is more rapid when the upstream sediment is less durable, as expected.

[42] This example illustrates how the efficiency of abrasion, as parameterized by α, controls the rate of fining downstream of an abrupt change in the input size distribution. The abrasion coefficient controls both the steady state mass of the coarse material as it arrives at the lithologic contact, and the rate of size reduction with distance. Also, because we assumed that the finer sediments are less durable, the downstream sediment mass equilibrates to a lower mass, thus reducing the mass component of the finer sediments in the bed load mixture and lengthening the distance over which the fining occurs.

3.1.2. Fining Along a Channel Network Mainstem

[43] We next consider downstream fining due to an abrupt reduction in the mean of the size distribution of entering sediment, in the setting of a real channel network, the upper Noyo River in Mendocino County, California (Figures 1, 2a, 2b, and 2c). In contrast to the previous example, we specify two very poorly sorted entering sediment size distributions (Figure 10a), both derived from log normal distributions but with the coarse tail of the coarser upstream distribution severely truncated (resulting in negative skew) and the fine tail of the finer downstream distribution severely truncated (resulting in positive skew). We assign α = 0.0001/m to the finer distribution and α = 0.00005/m to the coarser distribution. The lithologic contact is assumed to cross the watershed such that the more durable coarse sediment is supplied to all channel segments that are greater than 19 km upstream of the downstreammost point in the network (the "outlet"). Note that the modeled input grain size distributions are not based on field measurements, but rather are selected to illustrate how downstream fining might occur in a channel network.

[44] The upper Noyo River channel network and watershed topography are derived from overlaying the USGS blue line DLG onto a 10m DEM and extending the channel network by using a 40,000 m^2 channel initiation threshold. The tips of the channel network used here have been pruned to exclude channels steeper than 10%, because of the presumed dominance of debris flow sediment transport and valley incision in the steeper headwater channels [e.g., *Stock and Dietrich*, 2003; *Dietrich et al.*, 2003].

[45] For the outlet and for each of nine points midway between major tributary junctions along the main stem, we use a numerical routine to calculate the resulting grain size distribution and mass of the bed load. For each point of

analysis we calculate the width function and the coinciding incremental area function (Figures 2a and 2c show these functions for the outlet). The sediment loading for each upstream distance is obtained by summing the mass input of each incremental area (equation (24)), assuming a uniform erosion rate E of 0.1 mm/yr, and a rock density ρ_s of 2500 kg/m^3. From the mass loading and the appropriate grain size pdf by mass, we calculate the number of input particles in each size class. Finally, for each travel distance, the grain size reduction due to abrasion is calculated and the grain size distribution is obtained by summing over all upstream distances.

[46] Figure 10b shows the bed material grain size distributions for each of the nine nested subbasins and for the outlet. The downstream evolution of the median grain sizes is shown in Figure 10c, along with the downstream accumulation of drainage along the main stem. Where the channel is upstream of the shift in supply ($x > 19$ km, subbasins 7, 8 and 9), the bed load pdf is indistinguishable from the entering sediment. Downstream of the shift to the finer supply, the median grain size declines rapidly (Figure 10c), reflecting the gradual shift in the grain size distribution of the bed load mixture from the coarse to the finer supply. The bed load pdf at the outlet is not identical to the steady state bed load pdf that corresponds to the finer entering sediment distribution, however, for two reasons. First, $L_D^* \sim 52$ km for that distribution, so the fine supply component of the bed load is still evolving. Second, there is also a significant fraction of the bed load particles at the outlet which are derived from the coarse supply delivered in the distal portions of the watershed because $L_D^* \sim 125$ km for the coarser upstream distribution of entering sediment. All the coarse supply particles initially larger than about 5 mm are thus still part of the bed load mixture at the outlet, but their size has been greatly reduced by abrasion. As a result, the mean of the outlet distribution is somewhat smaller than the mean of the fine-grained supply, but the outlet distribution also has a slightly thicker tail in the coarse size classes.

[47] The downstream evolution of the bed load flux $M(x)$ is shown in Figure 10d. Mass increases rapidly and continuously in the upstream portion of the main stem profile (15 km $< x <$ 20 km), with no apparent effect from crossing the supply discontinuity at 19 km. Below $x =$ 15 km, however, the bed load flux drops to about half the peak value, reflecting the increased efficiency of abrasion (greater α) of the less durable downstream supply and the reduced rate of area accumulation downstream of the peak in the width function (Figures 2a and 2b).

3.2. Tributary Junctions

[48] The branching structure of channel networks should most strongly influence bed material grain size distributions at tributary junctions, where abrupt changes in the characteristics of sediment supply to the main stem channel are possible. Tributary junctions are commonly observed to be sites of infusions of coarse material, particularly where debris flows arriving from steep tributary channels are halted by high angle junctions with the main stem [e.g., *Howard and Dolan*, 1981; *Montgomery et al.*, 2003]. Where lateral sediment supply from adjacent hillslopes is intercepted by wide valley bottoms, pronounced downstream fining between tributary junctions has been observed [*Rice and Church*, 1998; *Rice*, 1998, 1999], although selective transport may be the dominant influence if there is net deposition [e.g., *Ferguson et al.*, 1996; *Hoey and Bluck*, 1999]. Here we consider how particle abrasion and spatial variability in sediment supply can affect the magnitude of perturbation of the main stem bed material at tributary junctions, for the case of no net deposition over geomorphic timescales.

3.2.1. Individual Tributary Junctions

[49] If the two streams are transporting the same bed load size distribution, composed of rocks of equal durability (i.e., same α), there will be no change in the main stem grain size distribution downstream, only a change in bed load mass flux. Where the size distributions of the bed load in each stream are not the same, the resulting change in main stem grain size (ΔD) will scale with the magnitude of the change in bed load mass flux in the main stem (ΔM) after the addition of the tributary input. Figures 11a and 11b show schematic diagrams of changes in bed load mass flux and median grain size across a tributary junction. For this simple example, the main stem contribution of bed load flux (M_m) is assumed to come from the upstream supply of sediment from the valley side slopes, and is shown as constant in Figure 11 although we might expect it to change over the scale of the diagram due to variations in the local side slope supply rate. We first consider changes in only the bed load mass flux, and then changes in grain size.

[50] Because particle abrasion converts a significant fraction of the bed load material supplied upstream to silt, the fractional change in bed load mass immediately downstream of the junction ($\Delta M/M_m$) will not scale simply with relative drainage area, but rather should depend on the upstream lengths of the two channels (L_{trib} and L_{ms}). For the case of spatially uniform erosion rate in both the tributary and upstream main stem watersheds (i.e., uniform side slope supply for all channels), we can identify three classes of tributary junctions, scaled by the ratio of the upstream lengths of the two channels (L_{trib} and L_{ms}) to the mass equilibration length $1/\alpha$. The simplest case is where both channels have reached steady state bed load mass flux (i.e., $L_{trib} > 1/\alpha$; $L_{ms} > 1/\alpha$) and the flux doubles immediately downstream of the junction ($\Delta M/M_m \sim 1$). Where only the main stem mass has equilibrated ($L_{trib} < 1/\alpha$; $L_{ms} > 1/\alpha$), the fractional change in mass $\Delta M/M_m \approx 1 - e^{-\alpha L_{trib}}$ and where both stream lengths are less than $1/\alpha$, the fractional mass change $\Delta M/M_m \approx (1 - e^{-\alpha L_{trib}})/(1 - e^{-\alpha L_{ms}})$. As shown in Figure 11a, the mass perturbation will decay exponentially downstream, because the sediment resupply from side slope erosion is only sufficient to sustain the original main stem bed load flux M_m. The length scale for the decay of the mass is simply $1/\alpha$, the distance over which 95% of the tributary mass will have been abraded to silt.

[51] Where tributaries transport a coarser size distribution than the main stem, the mean size distribution of the sediment mixture immediately downstream will be approximately equal to the average of the two distributions, weighted by their relative mass contribution. For lognormal pdfs of bed load sediments we can use a simple mixing relation to calculate the change in mean grain size ($\Delta D = D_{mix} - D_m$) as a function of the mean grain sizes of

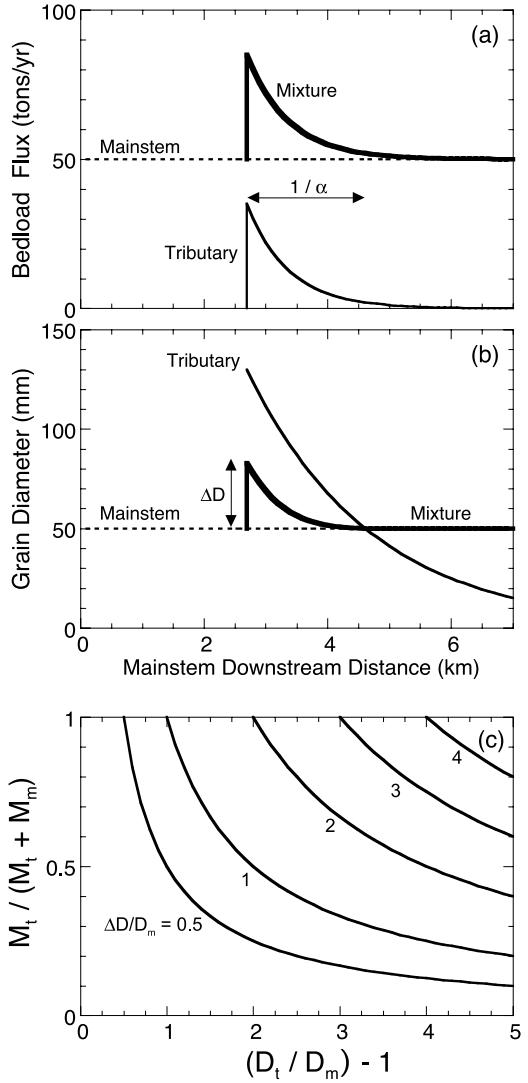

Figure 11. Perturbations to main stem bed load flux and mean grain size at individual tributary junctions. (a) Variation in bed load mass flux with downstream distance of the main stem sediments supplied from upstream and the valley side slopes M_m, the sediments supplied by the tributary M_t, and the resulting sediment mixture M_{mix}. (b) Variation in mean grain size with downstream distance of the tributary D_t and mainstream D_m sediments and the resulting sediment mixture D_{mix}. (c) Contours of constant relative grain size perturbation $\Delta D/D_m$ as a function of the mass fraction of tributary sediments $M_t/(M_t + M_m)$ and ratio $(D_t/D_m) - 1$ at the tributary junction.

the main stem (D_m) and tributary (D_t) and the bed load mass of the two streams, M_m and M_t respectively, as

$$\frac{\Delta D}{D_m} = \left(\frac{M_t}{M_t + M_m}\right)\left(\frac{D_t}{D_m} - 1\right) \tag{25}$$

Note the constraint that $0 \leq [M_t/(M_t + M_m)] \leq 1$.

[52] Figure 11c shows solutions of equation (25) as contours of constant $(\Delta D/D_m)$, for the relative grain size range of $1 < D_t/D_m < 5$, and for all possible mass ratios. Small perturbations in grain size (e.g., $\Delta D/D_m = 0.5$) occur when the tributary mass contribution is small but the grain size difference is large, or when the grain size difference is small but the tributary mass is large. For large grain size changes (e.g., $\Delta D/D_m = 4$) both the mass contribution and the grain size difference must be large. The distance over which the grain size perturbation decays $L^*_{\Delta D}$ will scale with the travel distance required to abrade the coarser tributary sediments down to the size of the main stem inputs from upstream

$$L^*_{\Delta D} = \frac{1}{\alpha} \ln\left(\frac{D_t}{D_m}\right) \tag{26}$$

These results are consistent with the field observations and qualitative arguments of *Knighton* [1980].

3.2.2. Multiple Tributary Junctions

[53] If the spacing between tributary junctions is small relative to the tributary mass decay length scale $1/\alpha$ then the effects on the main stem of an individual tributary sediment injection will be superposed on the partially decayed legacy of upstream tributary junctions. Conversely, if $1/\alpha$ is much smaller than the distance between tributary junctions, then the bed load sediments of large segments of the main stem channel will reflect only the local valley side slope supply, with no hint of disruptions due to upstream tributary junctions. Here we explore the range of potential bed load mass flux variability along the main stem of the Noyo River, by varying the rock durability parameter α over three orders of magnitude.

[54] For this calculation we selected the 26 tributaries entering the Noyo River main stem along its ~20 km course that have a contributing area greater than 0.38 km^2. Every junction is associated with a main stem channel length segment. (Each channel segment arc has a unique length, the average is ~100 m.) For the remaining nontributary channel segments we then used the length-weighted average incremental drainage area addition (a = 0.68 km^2/km), and equation (24), to calculate an average valley side slope loading rate (q_{vss}) of 0.17 tons/yr km, and assumed that this value applies to the main stem and each tributary above its confluence with the main stem. For each tributary we measured the upstream maximum travel distance within the subnetwork to obtain L_{trib} and calculated the bed load mass flux of the tributary M_t and the main stem M_m just upstream of the confluence using a simplified form of equation (15)

$$M(L) = \frac{q_{vss}}{3\alpha}\left(1 - e^{-3\alpha L}\right) \tag{27}$$

For $L = 1/\alpha$ the bed load flux approaches the steady state value $M_{ss} \approx q_{vss}/3\alpha$.

[55] Figure 12 shows a dramatic difference in the predicted pattern of bed load flux variation along the main stem, due to the combination of tributary and main stem valley side slope inputs, as we vary α from 0.01/m (very weak rocks) to 0.00001/m (very hard rocks). When the bed load sediments break down very rapidly (α = 0.01/m; Figure 12a), the bed load flux of both the tributary and the main stem is at the steady state side slope supply value M_{ss}, and the main stem flux doubles at each tributary junction. The doubling is short-lived, however, as the perturbation to the main stem bed load flux decays very rapidly. For this end-member case of very weak rocks, the bed load flux at any point along the main stem channel is

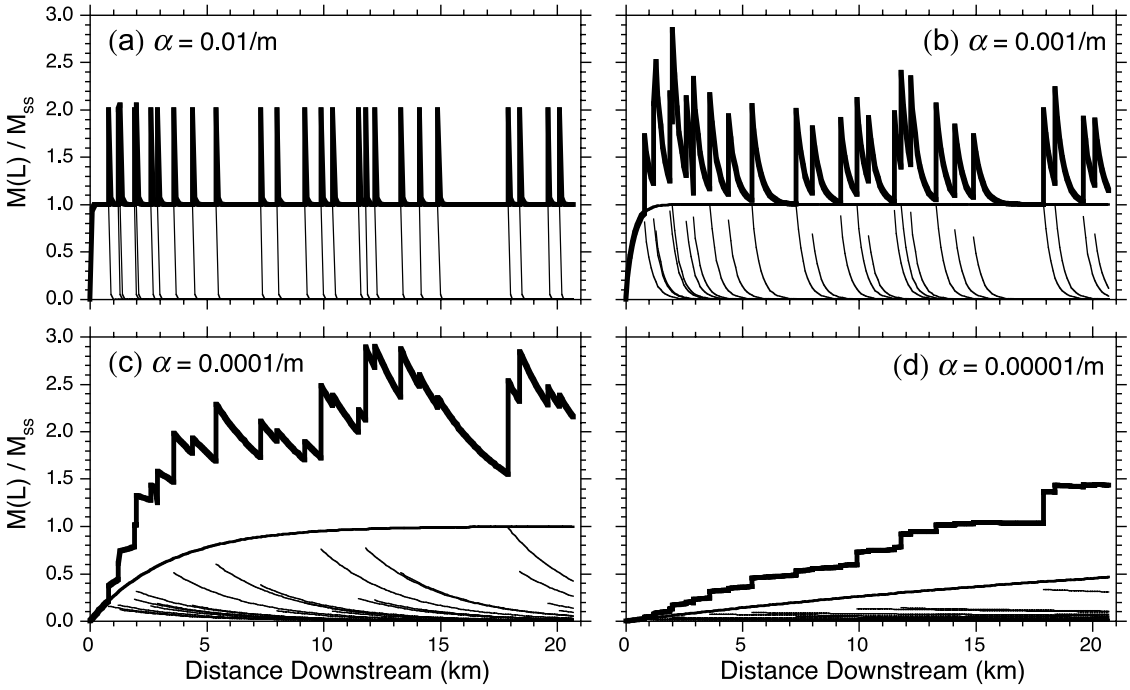

Figure 12. Variation in bed load mass flux along the Noyo River main stem due to tributary sediment inputs for various values of the abrasion coefficient α. Mass flux $M(L)$ is normalized by the steady state mass flux M_{ss} for uniform side slope input $q(L) = 170$ ton yr^{-1} km^{-1}. Thickest line shows total mass flux M_{mix}, which is a sum of the tributary bed load M_t (thinnest lines, lower portion of each panel) and the main stem bed load due to valley side slope supply M_m (medium thick line, which asymptotes to M_{ss}).

essentially independent of both the drainage area of any individual tributary basin and the spacing between tributary junctions.

[56] Differences among tributary junctions begin to emerge when we consider moderately weak rocks (α = 0.001/m; Figure 12b). The perturbation decay length scale $1/\alpha$ is an order of magnitude longer than in the previous case, longer than the spacing between most adjacent confluences. Only two gaps between junctions (at $L_m \sim 7$ and 17 km) are large enough for the mass flux to drop back to the steady state value M_{ss}. Some of the smaller tributary basins have $L_{trib} < 1/\alpha$ and thus contribute less than M_{ss} to the bed load mixture, however, even the smallest subbasins have reached ~70% of the steady state flux. As a result, there is some minor variability in the size of the main stem flux perturbation, mostly due to the occurrence of some closely spaced confluences, where the tributary mass superposition is significant.

[57] Increasing rock durability by another order of magnitude (α = 0.0001/m; Figure 12c) fundamentally alters the pattern. For these moderately hard sediments, the tributary decay distance $1/\alpha$ is greater than all interjunction distances, and much greater than most, so that tributary superposition elevates the average main stem flux to roughly double M_{ss}. Pronounced differences emerge in the magnitude of mass perturbations caused by tributaries of differing sizes. Large tributaries, particularly those entering downstream of a long unbranched length (e.g., $L_m \sim 18$ km), cause the largest change in bed load flux, while small tributaries (e.g., $L_m \sim$ 8 km) result in very small changes in flux, but do have the effect of resetting the decay and prolonging the spatial duration of elevated bed load mass.

[58] For the end-member case of very hard rock (α = 0.00001/m; Figure 12d), the decay distance $1/\alpha$ is much longer than the entire modeled profile length so that bed load mass flux, due to both tributary and valley side slope supply, increases steadily, roughly in proportion to the increase in upstream drainage area. Individual confluences result in step function increases in bed load, with no portions of the profile showing downstream decline in flux. At the downstream end of the 20km profile, bed load mass due to valley side slope supply has grown to about half of the steady state side slope flux M_{ss} of 6000 ton/yr. Because of abrasion, however, the total mass flux is only 20% of the total upstream coarse sediment supply for this 160 km^2 basin.

3.3. Width Function

[59] We now consider how the branching structure of channel networks, as represented by the width function, might influence bed material grain size distributions and bed load mass flux at any single point within the network. The width function (Figure 2a) is the distribution of travel distances to a downstream point, and its low-frequency component broadly reflects the shape of the drainage basin [e.g., *Rinaldo et al.*, 1995], and at finer scales reflects the internal branching structure of the network [e.g., *Troutman and Karlinger*, 1984; *Rinaldo et al.*, 1993]. Because size reduction by abrasion is a simple function of travel distance, it is reasonable to expect that basins with differing width functions will have different bed material characteristics. Moreover, because the width function is a function of length, its characteristic scales of variability in the low-frequency component (depicting the shape of the basin) and its high-frequency components (depicting the fractality of

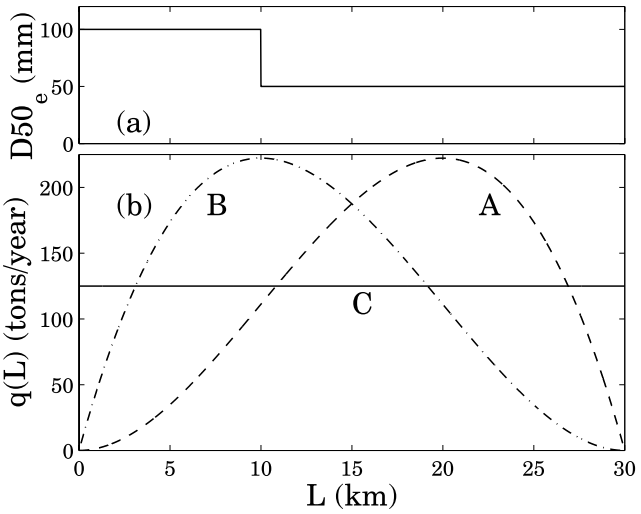

Figure 13. Variable entering sediment size and load rates for numerical experiments with the width function. (a) Entering grain size used only in experiment of Figure 16 showing abrupt downstream fining of supply at L = 10 km. (b) Three different load rate functions (A, B, and C), where functions A and B mimic the lateral load that would enter the main stem in two different basins of width functions having shapes similar to A and B and C is equivalent to a constant width basin. The outlet of the basin is at distance L = 30 km.

the branching structure), relative to the fundamental abrasion length scale $1/\alpha$, will influence both the grain size pdf and mass of bed load sediment at the outlet of the basin. Note that if the erosion rate E and the incremental drainage area per unit channel length a are uniform across the basin, the width function would be equivalent to the incremental sediment loading function $q(L)$.

[60] Here we report the results of three numerical experiments in which we compare three different loading functions (equivalent to width function shapes), shown in Figure 13b. Note that the basin outlet is located at L = 30 km, so that the upstream is on the left of Figure 13 and the downstream on the right, the reverse of the conventional representation of the width function. The basin that corresponds to width function "A" would have a large fraction of the drainage area located close to the outlet. The most common basin shape, which narrows toward the outlet and only has a small area fraction close to the outlet, would correspond to "B." Width function "C" is equivalent to a long, narrow basin without significant branching structure.

3.3.1. Effect of Variance of the Entering Sediment pdf

[61] In the first experiment we varied the spread of the distribution of entering sediment to see how the basin shape would affect the resulting pdf of bed load sediment at the outlet. We used the same four pdfs of entering sediment, one of constant size and the other three lognormal, as in Figure 6 and Table 1. Figure 14 shows the steady state bed load sediment pdfs of the four entering sediment pdfs, for each of the three width functions. Two clear patterns are apparent.

[62] First, there is a systematic difference in the extent to which the bed load pdfs are different from the entering pdfs,

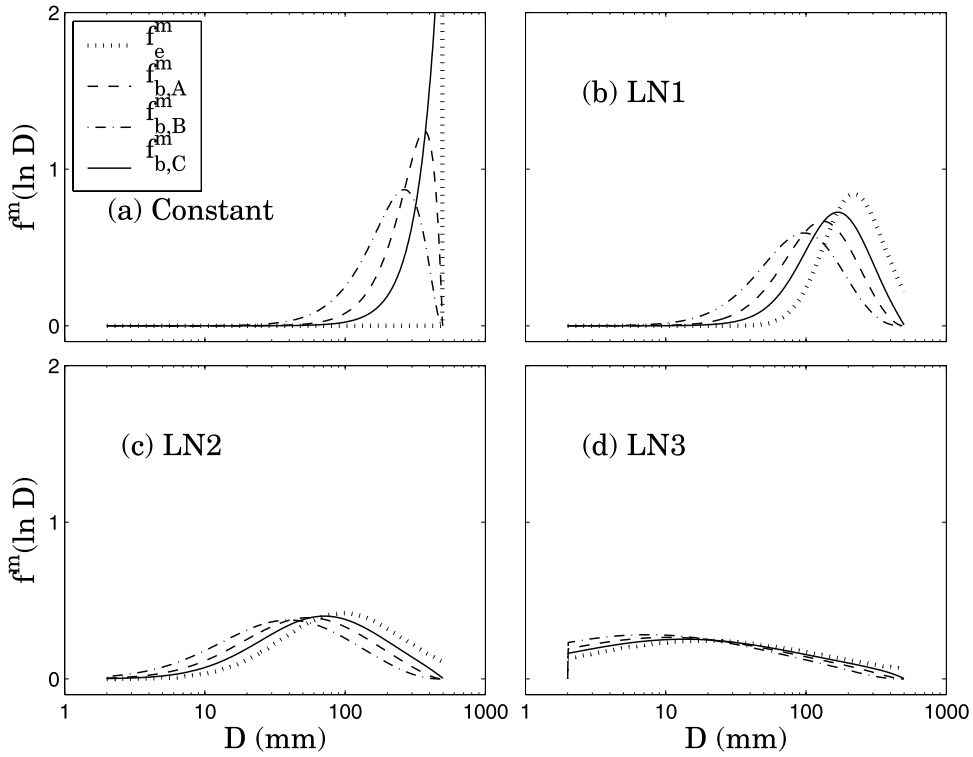

Figure 14. Comparison of the pdfs of entering and steady state bed load diameter by mass for the three different load functions A, B, and C given in Figure 13 for four input pdfs of varying width (Table 1): (a) a constant size of entering sediment D_e = 500 mm, (b) LN1, (c) LN2, and (d) LN3.

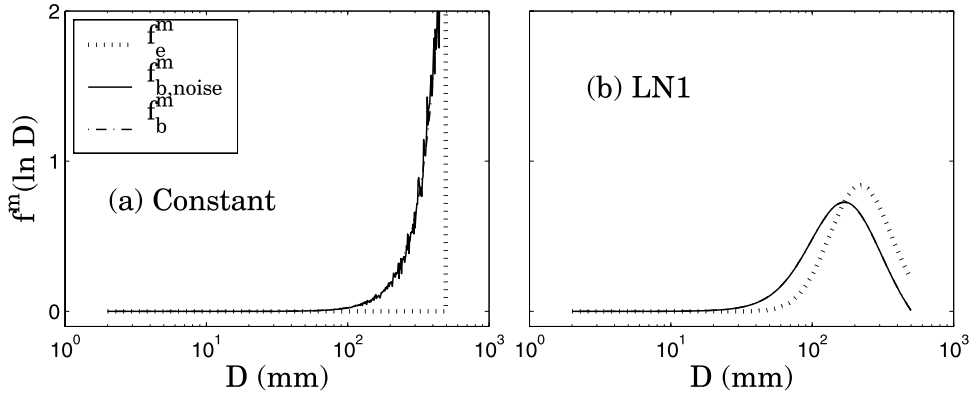

Figure 15. Comparison of pdfs of entering sediment diameter by mass $f_e^m(\ln D_e)$ (dashed lines) to those of the steady state pdfs by mass of the bed load $f_b^m(\ln D)$ (solid lines) for (a) the constant size and (b) the narrow width pdf LN1 for a constant load function with 10% Gaussian noise. Note how the fluctuations in the load are dissipated when there is even modest width to the pdf of the entering sediment.

which is most apparent for the case of a single uniform entering grain size (Figure 14a). Width function C is the least modified, B is the most modified, and A is intermediate. This pattern can be explained by considering the area under the loading curves in Figure 13 and recognizing that for this example the travel distance required to convert the coarsest entering grains to sand ($L^* = 27.6$ km) is the same order of magnitude as the length of the simulated basins. The loading nearest the outlet ($L \sim 30$ km) will have the greatest influence on the bed load pdf, particularly for the pdf by mass because of the cubic dependence of mass on grain diameter. Width function 'C' has the largest near-outlet loading and thus produces a bed load pdf that most closely resembles the entering sediment pdf, while B has very little loading over the nearest 5 km to the outlet so much more of its sediments have been reduced in size by abrasion.

[63] Second, as the variance of the entering sediment pdf increases, the effect of the differing width functions decreases. For the distribution with the largest variance, LN3 (Figure 14d), there is almost no difference between the width functions A, B and C, implying a very weak dependence of the bed load sediment pdf on the basin shape and the branching structure of the river network. Width function C is equivalent to the analytical result discussed above for a constant load q (Figure 6). The effect of the asymmetrical loading is to allow abrasion to modify the entering pdf slightly more extensively, by suppressing the resupply of the fresh entering pdf near the outlet. This near-outlet resupply reduction is greater for the case of B than A, thus the B bed load pdfs are somewhat finer than the others, even for the largest variance (Figure 14d). Overall, however, it can be said that for highly unsorted sediment entering from the hillslopes, the structure of the river network does not leave its imprint on the bed load sediment size downstream.

3.3.2. High-Frequency Variability in Sediment Supply and Travel Distances

[64] For the problem under consideration, i.e., bed material grain size distribution and bed load mass flux, the fractality of the river network enters into the picture in two distinct but related ways. First, the sediment supply to the main stem can be considered proportional to the incremental drainage area per unit channel length, which is known to exhibit high-frequency variability (e.g., Figure 2c). Second, the travel distances to the outlet, which control the size reduction by abrasion, are also known to exhibit high-frequency variability and are imprinted in the high-frequency fluctuations of the width function, which have been extensively studied in the literature [e.g., *Rinaldo et al.*, 1993].

[65] These two sources of high-frequency variability are bound to influence the bed load size distribution but it is not obvious how. Here we have performed a numerical experiment in which a channel reach of 30 km receives a lateral load with high-frequency fluctuations mimicking those of the incremental area per unit channel length of Figure 2c. This load function $q(L)$ is created by superimposing Gaussian white noise on a constant load q, and the standard deviation of the noise is set as 10% of the constant load.

[66] Figure 15 shows the steady state bed load pdfs by mass for the case of constant entering sediment load (solid lines) and load with high-frequency fluctuations superimposed (dashed lines) and for two pdfs of entering sediment (constant size and narrow-width lognormal). We observe that only in the case of a single input sediment size do the high-frequency fluctuations in the load get propagated to the pdf of the bed load sediment. In all other cases, the high-frequency variability of the input sediment is effectively eliminated even by the most modest variance of input sediment (LN1 in Figure 15b). Fluctuations of long memory or long-range dependence and power law distributions can be easily tested and will be the subject of subsequent research.

3.3.3. Effect of the Abrasion Length Scale $1/\alpha$

[67] As previous examples have illustrated clearly, the rock durability parameter α sets the length scale for the downstream propagation of signals created by spatial variability in the rate and grain size of sediments supplied to the channel network. Here we investigate how this fundamental length scale modulates the influence of the upstream basin shape on the bed load sediments passing the outlet. For this experiment we use the simple pdf of a single entering grain size, and impose an abrupt shift 20 km upstream of the outlet (Figure 13a), from $D_e = 100$ mm upstream to $D_e = 50$ mm downstream; rock durability is assumed equal for both entering sizes. To simulate the range of possible outcomes for rocks ranging in strength from

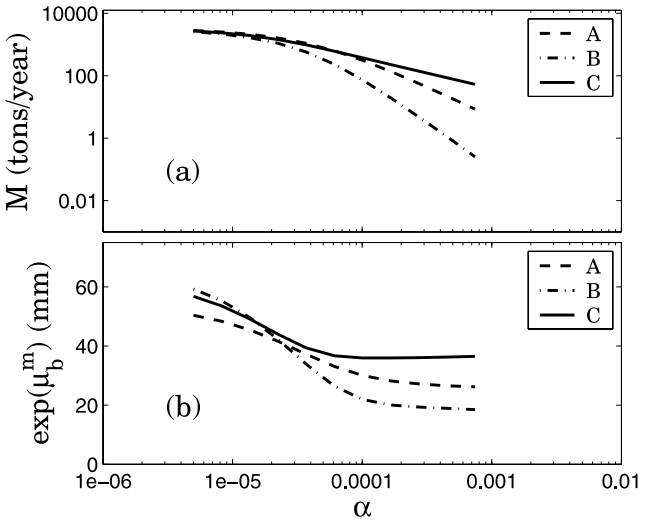

Figure 16. (a) Mass flux and (b) geometric means of the bed load sediment for the load functions A, B, and C of Figure 13 as a function of the abrasion coefficient α.

very hard to very weak we vary α through almost three orders of magnitude.

[68] Figure 16a shows the variation in bed load mass flux for the three basin shapes (A, B, and C, Figure 13) over the range of rock durability. For the hardest rocks ($\alpha \approx 0.00001$/m), there is no significant difference between the three width functions, abrasion is so inefficient that the mass flux scales simply with the area under the width function curves (Figure 13), which is the same for each basin shape. As rock durability declines (greater values of α) the bed load mass flux out of each basin is reduced, due to the increased mass transfer from bed load to suspended load by abrasion upstream of the outlet. The reduction in bed load flux with increasing α is most pronounced for basin B, and least for basin C because of the increased importance of the sediment input rate from the portion of the basin located close to the outlet. For the weakest rocks simulated ($\alpha = 0.001$/m), the length scale for mass equilibration with the local supply rate is approximately 1% of the basin length; virtually all gravel and coarser material supplied to the channel network by hillslopes is ground to silt before passing the outlet point. The modeled step function fining in entering sediment grain size at 20 km from the outlet does not significantly affect the bed load mass reaching the outlet, even when the rocks are very durable (low values of α).

[69] The effect of varying rock durability on the mean grain size of the bed load grain size distributions at the outlet is shown in Figure 16b, for the three width function shapes. When the rocks are very resistant to abrasion ($\alpha \approx 5 \times 10^{-6}$/m), all three width function shapes deliver a relatively coarse mean grain size to the outlet, because the coarser 100mm particles supplied from upstream retain significant mass at the outlet despite their long travel distance. The mean delivered by width function shape A is less coarse than the means for the other two shapes because A has about half as much area under the loading curve upstream of the shift in input sizes as the other two width functions. As rock durability decreases (α increases), the mean grain size for all width functions becomes smaller because the downstream finer supply begins to dominate. For the weakest rocks the mean grain size is no longer a mix of the coarse and fine supplies because all the coarse grains are ground to silt before reaching the outlet. Instead, for this example, the variation between width functions in the mean grain size depends on the rate of change of the loading nearest the outlet. Width function C has a uniform load and thus delivers the steady state bed load size distribution that evolves from the single size input of 50 mm. Width functions A and B deliver finer sediments to the outlet than 'C' because the load rates are declining, particularly for B, such that the resupply near the outlet does not fully offset the size reduction of the sediments supplied just upstream.

[70] This example illustrates that the basin shape and branching structure can influence grain size distributions at a downstream point in the network, but the effect of variable width function shape is strongly modulated by the efficiency of particle abrasion.

4. Discussion

[71] Contrary to our initial expectations, channel network structure alone does not appear to meaningfully influence bed material grain size distributions. Rather, basin shape and the internal branching pattern can either amplify or dampen the effects of spatial variability in the size of sediments delivered to channels by hillslopes. In the absence of strong spatial variations in input sizes, rock durability or erosion rate, downstream abrasion and continuous replenishment of coarse sediment supply combine to drive the channel system to a steady state bed load flux and size distribution independent of network structure. As illustrated above, the influence on bed load variability of channel network properties such as the width function and the spacing between tributary junctions depends on the fundamental length scale imposed by particle abrasion. Sediments derived from weak rocks wear to silt over such a short distance that the evidence of the upstream network structure is effectively destroyed. The most abrasion-resistant rocks require such long distances to wear significantly that differences in travel path to a point don't result in strong differences in grain size. It is for sediments of intermediate rock durability that we expect the greatest variability in bed load mass, because fluctuations in valley side slope supply (Figure 2c), tributary junction spacing (Figure 12c), and basin width are most likely to occur at length scales that allow for significant wear but not complete destruction of sediments supplied from upstream.

[72] Our results offer a new perspective on the debate over the cause of downstream fining. As *Rice* [1999] and *Heller et al.* [2001] have previously suggested, abrasion alone will not cause fining when there is active resupply from local sources, which there must be over a sufficiently long timescale. Thus observed patterns of fining in actively incising terrain may be due to a combination of relatively short-term ($\sim$1–10 ka) selective transport of finer bed load material and net deposition of coarser grains, and a systematic landscape-scale gradient in the size distribution of sediments delivered by hillslope processes. This second scenario has been previously suggested by *Pizzuto* [1995] in modeling the pattern of fining first reported by *Brush* [1961] in an Appalachian watershed with strong lithologic contrasts.

[73] The tendency for bed load mass flux to approach a steady state value has important implications for understanding the influence of sediment supply on river incision and landscape evolution. From our analysis and simulations, a picture emerges of the mobile bed load mass as a silt factory, which efficiently adjusts its productivity to match the rate of coarse sediment input. Contrary to the common assumption that bed load mass flux increases steadily with increasing drainage area, our results suggest that bed load mass equilibrates with hillslope supply over a length scale of $1/\alpha$, after which it becomes independent of drainage area. For spatially uniform sediment inputs, the fraction of the total load that travels in suspension should then increase downstream while the bed load fraction is reduced. Discharge obviously does scale with drainage area [e.g., *Leopold and Maddock*, 1953; *Gupta et al.*, 1996], so that we might expect the ratio of bed load sediment supply to transport capacity to decrease downstream, resulting in greater exposure of bedrock in the channel bed [*Sklar and Dietrich*, 1998, 2004] and perhaps a less rapid growth in the bedrock channel width with downstream distance [e.g., *Montgomery and Gran*, 2001; *Whipple*, 2004]. If the slope of bedrock rivers depends on the bed load sediment supply relative to transport capacity [*Sklar and Dietrich*, 2006], then tributary junctions where $L_{trib} < 1/\alpha < L_m$ might form convexities in the main stem profile, even in the absence of grain size variations [*Sklar and Dietrich*, 1998]. This would occur because the marginal increase in main stem load downstream of the junction is greater than the increase in discharge, requiring a steeper slope than upstream of the junction to maintain partial exposure of bedrock and active bed incision. In the extreme case, hanging valleys could result where tributaries with high bed load sediment loads relative to available discharge cannot incise rapidly enough to keep up with main stem channels that have abundant discharge but only limited bed load flux. Because bedrock lithology and rainfall are generally heterogeneous at length scales equal to or less than the abrasion length scale $1/\alpha$, feedbacks between hillslope sediment supply, bed load composition, and bedrock incision may be important in driving dynamic evolution of the drainage network structure itself.

[74] We can also use our results to speculate about the influence of rock durability on the timescale of adjustment of bed material to shifts in sediment supply. Temporal variations in the size distribution or rate of sediment supply might be caused at longer timescales by changes in hillslope sediment production processes brought on by changes in climate [e.g., *Inman and Jenkins*, 1999] or erosion rate [e.g., *Peizhen et al.*, 2001] or exhumation of different lithologies [e.g., *Clapp et al.*, 2000], and at shorter timescales by shifts in land use [e.g., *Doyle and Shields*, 2000] or simply the temporal variability in sediment delivery inherent in magnitude-frequency relations of different hillslope sediment production and transport processes (e.g., landsliding versus soil creep). The timescale of bed response τ should scale with the ratio of the abrasion length scale L_D^* to the average sediment velocity u_s

$$\tau \approx \frac{L_D^*}{u_s} = \frac{\ln(D_{\max}/D_{\min})}{\alpha u_s} \tag{28}$$

Annual downstream transport distances for gravel- and cobble-sized grains are of order 100m [e.g., *Hassan et al.*, 1991] so, for example, if $D_{\max} = 100$ mm, $\alpha = 0.0002$/m, and $L_D^* \sim 20$ km, then approximately $\tau = 200$ years are required for the evidence (in the bed load) of the prechange sediment supply to be destroyed. For harder, coarser rocks (e.g., $D_{\max} = 500$ mm, $\alpha = 0.00005$/m, $L_D^* \sim 100$ km), $\tau = 1000$ years, while for weaker rocks producing a finer grained supply (e.g., $D_{\max} = 50$ mm, $\alpha = 0.005$/m, $L_D^* \sim 0.6$ km) τ might be less than a decade. This back of the envelope calculation suggests that the composition of active river bed sediments adjusts quite rapidly to temporal changes in sediment supply characteristics, and that significant supply from long-term storage reservoirs in floodplains, terraces and fans is required for a previous sediment supply regime to maintain its influence over contemporary bed materials.

[75] The predicted tendency for the mass flux to reach a steady state $M_{ss} = q/3\alpha$ after a distance L_D^* downstream of the most distant channel head may provide a simple method for estimating long-term average bed load in a field setting. This would require estimating the average hillslope sediment production rate, the fraction of the hillslope sediment supply coarse enough to move initially as bed load, and a representative value for the abrasion coefficient α. The local topography and channel network structure can then be used to determine the incremental area per unit channel length and the location of L_D^*. Estimates of M_{ss} might be useful in a wide variety of practical and theoretical contexts, from predicting the gravel fraction of reservoir sediment deposits [e.g., *Willis and Griggs*, 2003] to interpreting longitudinal profile concavity [e.g., *Sklar and Dietrich*, 2006].

[76] Caution in sampling bed load material sediments ($D \gg 2$ mm) for cosmogenic radionuclide estimates of watershed-scale erosion rates [e.g., *Reusser et al.*, 2004; *Wolkowinsky and Granger*, 2004] is also suggested by our results. The more efficient the abrasion process (greater α), the less the bed material will reflect watershed-wide sediment supply conditions. For the weakest rocks, only the most local sources will be represented in a sample of bed load material. Even for the hardest rocks, for sufficiently large basins abrasion will tend to destroy the signal carried by coarse sediments entering in the distal portions of the watershed. Although not considered here, suspended material is also subjected to abrasion during transport, so that samples of sand may also be biased toward the local supply.

[77] Two major priorities for further research are suggested by this work. First, the overarching question of what controls the grain size distribution of sediments supplied by hillslopes to the channel network encompasses a rich set of questions about the roles of, and feedbacks between, bedrock lithology, climate, erosion rate, and hillslope sediment production and transport processes, and represents a broad frontier in process geomorphology. Second, and more narrowly important, we need an improved basis for quantifying the rate of abrasion of bed load sediments in rivers. The Sternberg abrasion coefficient α sets the scale for bed material evolution, yet this model parameter remains somewhat of a black box. Improved models for grain size reduction that account for splitting as well as abrasion may also change the predicted extent and pattern of grain

size evolution with downstream transport. Methods are needed both for translating experimental measurements of size reduction and calibrations of α to specific field contexts, and for distinguishing in the field the particle size reduction due to abrasion from other sources of spatial variability in bed material grain size.

5. Conclusion

[78] We began this study with the thought experiment of standing next to a gravel river bed in actively incising terrain, looking upstream, and asking how the distribution of fluvial travel distances and transport pathways imposed by the drainage network structure should affect the size distribution and flux rates of the bed material at this point. We conclude that we need to look farther upstream, out of the channel and up to the hillslope source of sediments, to understand the spatial trends and variability in bed load size distributions. The processes of particle size reduction by abrasion during transport, and resupply of the entering sediment by local sources, combine to drive the bed load transport system toward two related equilibria: a steady state grain size distribution that differs little from the hillslope supply, and a steady state mass flux that abrades bed load mass to silt at the rate of resupply of coarse sediment. The efficiency of abrasion, parameterized by α, the exponent in the exponential abrasion rate law, sets the fundamental length scale for bed material adjustment to spatial and temporal changes in sediment supply characteristics, whether those changes are due to emergent properties of the channel network structure such as tributary junction spacing, or locally contingent factors introduced by lithologic contacts or changes in land use. Rock durability, the dominant factor in abrasion efficiency, then controls where and how spatial variation in sediment supply is expressed in the bed load size distribution and mass flux across the landscape. This work highlights the need to greatly improve our understanding of what controls the size distribution of sediments produced and delivered to channel networks by hillslopes.

Appendix A: Derivation of $f_b^g(D)$

A1. Constant D_e

[79] We use a derived distribution approach by which the pdf of a transformed random variable $Y = g(X)$ is easily seen to be given in terms of the pdf of X, $f_X(x)$, as

$$f_Y(y) = f_X(x)/|g'(x)| \tag{A1}$$

where $g'(x)$ is the derivative of $g(x)$. The relevant transformation here is Sternberg's law which transforms a distance, and thus lateral load over that distance, to a grain size D by

$$D(x) = D_e e^{-\alpha x} \tag{A2}$$

We note from (A2) that $dD/dx = -\alpha D$ and thus for a uniform lateral load of constant rate q (kg km^{-1} yr^{-1}) we can write that

$$f_b^g(D) = \frac{1}{L} \Big/ \left|\frac{dD}{dx}\right| = \frac{1}{\alpha D L} \tag{A3}$$

A2. The pdf of Entering Sediment $f_e^g(D_e)$

[80] The last formula (A3) can be generalized to the case for which the entering sediment is distributed according to a probability distribution by grain $f_e^g(D_e)$.

[81] Let us first assume that the length of the channel L is such that

$$L > L^*_{D,p} = \frac{1}{\alpha} \cdot \ln\left(\frac{D_{\max,p}}{D_{\min}}\right) \tag{A4}$$

i.e., the bed load distribution has reached its steady state. The entering sediments with size in the range $[D_e, D_e + dD_e]$ result in the following number of grains at distance L:

$$q \cdot f_e^g(D_e) dD_e \times L^*_{D_e} = q \frac{1}{\alpha} \cdot \ln\left(\frac{D_e}{D_{\min}}\right) f_e^g(D_e) dD_e \tag{A5}$$

since the corresponding "active" part of the channel ranges from the distance $L - L^*_{D_e}$ down to the distance L. The total number of grains is given by

$$\int_{D_{\min}}^{D_{\max,p}} q \frac{1}{\alpha} \cdot \ln\left(\frac{D_e}{D_{\min}}\right) f_e^g(D_e) dD_e \tag{A6}$$

and the relative weight of the entering sediments with size in $[D_e, D_e + dD_e]$ is then

$$p(D_e) = \frac{\ln\left(\frac{D_e}{D_{\min}}\right) f_e^g(D_e) dD_e}{\int_{D_{\min}}^{D_{\max,p}} \ln\left(\frac{D_e}{D_{\min}}\right) f_e^g(D_e) dD_e} \tag{A7}$$

[82] These bed load grains, (abraded from input sediments with size $[D_e, D_e + dD_e]$) are distributed with the following conditional pdf:

$$f_b^g(D|D_e) = \frac{1}{D \ln(D_e/D_{\min})} \tag{A8}$$

and thus the pdf of the bed load sediment is given by

$$f_b^g(D) = \int_{D_{\min}}^{D_{\max,p}} f_b^g(D|D_e) p(D_e) dD_e \tag{A9}$$

Simple calculations eventually lead to

$$f_b^g(D) = \frac{1}{D} \cdot \frac{\int_D^{D_{\max,p}} f_e^g(D_e) dD_e}{\int_{D_{\min}}^{D_{\max,p}} f_e^g(D_e) \ln\left(\frac{D_e}{D_{\min}}\right) dD_e} \tag{A10}$$

for $D_{\min} \le D \le D_{\max,p}$. The computation of the bed load sediment pdf in the nonsteady state case is similar and results in equation (14) in the text.

Appendix B: Derivation of $M(L)$

[83] The incremental mass change $dM(L)$ in a length of stream dL is given as

$$dM(L) = qdL - 3\alpha M(L)dL \tag{B1}$$

where the first term in the right hand side is the entering mass over a distance dL and the second term is the lost mass by abrasion. This second term is derived by noting that each grain of size D_e entering at $L = 0$ becomes $D_i = D_e e^{-\alpha L}$ at distance L, and its mass $M_i = D_e^3 e^{-3\alpha L}$; thus the mass lost to abrasion for this grain is $dM_{a,i}(L) = M_i e^{-3\alpha L}$ and the total mass lost to abrasion from all grains $M_a(L) = \sum dM_{a,i}(L) = M(L)e^{-3\alpha L}$ yielding the total mass lost due to abrasion $dM_a(L) = -3\alpha M(L)dL$. From (B1), we solve for $M(L)$ assuming initial condition $M(0) = 0$ to get

$$M(L) = \frac{q}{3\alpha}\left(1 - e^{-3\alpha L}\right), \qquad L < L_D^* \tag{B2}$$

[84] In the case of $L \geq L_D^*$, there do exist grains of initial size D_e that have been abraded to the size $D_{\min}$ and that are since washed out by the stream. At distance L, there are $N_e dL = q/kD_e^3\, dL$ such grains, since all grains with size $D_{\min}$ at distance L have entered the stream at the same (upstream) distance $L - L_D^*$. The corresponding lost mass is $N_e k D_{\min}^3\, dL = q(\frac{D_{\min}}{D_e})^3\, dL$. Equation (B1) then becomes

$$dM(L) = qdL - 3\alpha M(L)dL - q\left(\frac{D_e}{D_{\min}}\right)^3 dL \tag{B3}$$

whose solution is, since $M(L_D^*)$ is analytically known through (B2)

$$M(L) = \frac{q}{3\alpha}\left[1 - \left(\frac{D_{\min}}{D_e}\right)^3\right], \qquad L \geq L_D^* \tag{B4}$$

Note that for $L \geq L_D^*$ the bed load mass flux does not depend on L.

Notation

- a incremental drainage area per unit channel length ($km^2\ km^{-1}$).
- D bed load grain diameter (mm).
- D_e diameter of entering sediment (mm).
- $D_{\max}$ maximum bed load grain diameter; $D > D_{\max}$ is immobile (mm).
- $D_{\max(L)}$ grain diameter that will wear to $D_{\min}$ after traveling a distance L (mm).
- $D_{\max,p}$ maximum grain diameter having probability of nonexceedance p (mm).
- $D_{\min}$ minimum bed load grain diameter; $D < D_{\min}$ travels in suspension (mm).
- E erosion rate (mm yr^{-1}).
- $f_b^g(D)$ pdf of bed load grain diameter, frequency by number of grains.
- $f_b^m(D)$ pdf of bed load grain diameter, frequency by mass.
- $f_e^g(D_e)$ pdf of entering sediment diameter, frequency by number of grains.
- $f_e^m(D_e)$ pdf of entering sediment diameter, frequency by mass.
- $F_e^m(D_e)$ cumulative distribution of entering sediment diameter, by mass.
- k grain mass coefficient ($kg\ m^{-3}$).
- L downstream travel distance along channel (m or km).
- L_D^* travel distance to reach steady state bed load size distribution (m or km).
- $L_{D,p}^*$ distance to steady state size distribution, entering pdf truncated at p.
- L_M^* travel distance to reach steady state bed load mass flux (m or km).
- $L_{M,0.95}^*$ travel distance to reach 95% of steady state bed load mass flux (m or km).
- $M(L)$ bed load sediment mass flux ($kg\ yr^{-1}$).
- M_{ss} steady state bed load mass flux ($kg\ yr^{-1}$).
- N_e Number of entering grains per unit distance (m^{-1}).
- p probability of nonexceedance.
- q uniform sediment load entering river laterally ($kg\ m^{-1}\ yr^{-1}$).
- $q(L)$ spatially variable lateral sediment load ($kg\ m^{-1}\ yr^{-1}$).
- u_s annual average bed load particle velocity ($m\ yr^{-1}$).
- α abrasion coefficient (m^{-1}).
- α_h abrasion coefficient of hard rock (m^{-1}).
- α_w abrasion coefficient of weak rock (m^{-1}).
- ΔD change in mean main stem grain size across tributary junction (mm).
- ΔM change in main stem bed load mass flux across tributary junction ($kg\ yr^{-1}$).
- ρ_s sediment density ($kg\ m^{-3}$).
- τ timescale of bed response to changes in sediment supply.

[85] **Acknowledgments.** This work was supported in part by the STC program of the National Science Foundation (NSF) via the National Center for Earth-Surface Dynamics (NCED) under agreement EAR-0120914 and by NSF grant EAR-0345344. We thank Rob Ferguson and an anonymous reviewer for thoughtful comments that helped improve the clarity of the paper.

References

Adams, J. (1978), Data for New Zealand pebble abrasion studies, *N. Z. J. Sci.*, *21*, 607–610.

Adams, J. (1979), Wear of unsound pebbles in river headwaters, *Science*, *203*, 171.

Bittelli, M., G. S. Campbell, and M. Flury (1999), Characterization of particle-size distribution in soils with a fragmentation model, *Soil Sci. Soc. Am. J.*, *63*, 782–788.

Brush, L. M. (1961), Drainage basins, channels, and flow characteristics of selected streams in central Pennsylvania, *U.S. Geol. Surv. Prof. Pap.*, *282-F*, 175 pp., U.S. Gov. Print. Off., Washington, D. C.

Clapp, E. M., P. R. Bierman, A. P. Schick, J. Lekach, Y. Enzel, and M. Caffee (2000), Sediment yield exceeds sediment production in arid region drainage basins, *Geology*, *28*, 995–998.

Dietrich, W. E., and T. Dunne (1978), Sediment budget for a small catchment in mountainous terrain, *Z. Geomorphol. Suppl.*, *29*, 191–206.

Dietrich, W. E., D. Bellugi, L. S. Sklar, J. D. Stock, A. M. Heimsath, and J. J. Roering (2003), Geomorphic transport laws for predicting landscape form and dynamics, in *Prediction in Geomorphology*, *Geophys. Monogr. Ser.*, vol. 135, edited by P. Wilcock and R. Iverson, pp. 103–132, AGU, Washington, D. C.

Dodov, B., and E. Foufoula-Georgiou (2005), Fluvial processes and streamflow variability: Interplay in the scale-frequency continuum and implications for scaling, *Water Resour. Res.*, *41*, W05005, doi:10.1029/2004WR003408.

Doyle, M. W., and F. D. Shields Jr. (2000), Incorporation of bed texture into a channel evolution model, *Geomorphology*, *34*, 291–309.

Ferguson, R. I., T. Hoey, S. Wathen, and A. Werritty (1996), Field evidence for rapid downstream fining of river gravels through selective transport, *Geology*, *24*, 179–182.

Gilbert, G. K. (1877), *Report on the Geology of the Henry Mountains: Geographical and Geological Survey of the Rocky Mountain Region*, 160 pp., Gov. Print. Off., Washington D. C.

Gomez, V., B. J. Rosser, D. H. Peacock, D. M. Hicks, and J. A. Palmer (2001), Downstream fining in a rapidly aggrading gravel bed river, *Water Resour. Res.*, *37*, 1813–1823.

Gupta, V. K., S. L. Castro, and T. M. Over (1996), On scaling exponents of spatial peak flows from rainfall and river network geometry, *J. Hydrol.*, *187*, 81–104.

Hack, J. T. (1957), Studies of longitudinal stream profiles in Virginia and Maryland, *U.S. Geol. Surv. Prof. Pap.*, *294-B*, 97 pp.

Hassan, M. A., M. Church, and A. P. Schick (1991), Distance of movement of coarse particles in gravel bed streams, *Water Resour. Res.*, *27*, 503–511.

Heller, P. L., P. E. Beland, N. F. Humphrey, S. K. Konrad, R. M. Lynds, M. E. McMilan, K. E. Valentine, Y. A. Widman, and D. J. Furbish (2001), Paradox of downstream fining and weathering-rind formation in the lower Hoh River, Olympic Peninsula, Washington, *Geology*, *29*, 971–974.

Hoey, T. B., and B. J. Bluck (1999), Identifying the controls over downstream fining of river gravels, *J. Sediment. Res., Sect. A*, *69*, 40–50.

Hooke, R. L., and N. R. Iverson (1995), Grain-size distribution in deforming subglacial tills: Role of grain fracture, *Geology*, *23*, 57–60.

Howard, A., and R. Dolan (1981), Geomorphology of the Colorado River in the Grand Canyon, *J. Geol.*, *89*, 269–299.

Inman, D. L., and S. A. Jenkins (1999), Climate change and the episodicity of sediment flux of small California rivers, *J. Geol.*, *107*, 251–270, doi:10.1086/314346.

Jacobson, R. B., and K. B. Gran (1999), Gravel sediment routing from widespread, low-intensity landscape disturbance, Current River Basin, Missouri, *Earth Surf. Processes Landforms*, *24*, 897–917.

Knighton, A. D. (1980), Longitudinal changes in size and sorting of stream-bed material in four English rivers, *Geol. Soc. Am. Bull.*, *91*, 55–62.

Kodama, Y. (1994a), Downstream changes in the lithology and grain-size of fluvial gravels, the Watarase River, Japan: Evidence of the role of downstream fining, *J. Sediment. Res., Sect. A*, *64*, 76–85.

Kodama, Y. (1994b), Experimental study of abrasion and its role in producing downstream fining in gravel-bed rivers, *J. Sediment. Res., Sect. A*, *64*, 76–85.

Kuenen, P. H. (1956), Experimental abrasion of pebbles 2. Rolling by current, *J. Geol.*, *64*, 336–368.

Leopold, L. B., and T. Maddock (1953), The hydraulic geometry of stream channels and some physiographic implications, *U.S. Geol. Surv. Prof. Pap.*, *252*, 56 pp.

Lewin, J., and P. A. Brewer (2002), Laboratory simulation of clast abrasion, *Earth Surf. Processes Landforms*, *27*, 145–164.

Malarz, R. (2005), Effects of flood abrasion of the Carpathian alluvial gravels, *Catena*, *64*, 1–26.

Matsuoka, N., and H. Sakai (1999), Rockfall activity from an alpine cliff during thawing periods, *Geomorphology*, *28*, 309–328.

Menabde, M., and M. Sivapalan (2001), Linking space-time variability of rainfall and runoff fields on a river network: A dynamic approach, *Adv. Water Res.*, *24*, 1001–1014.

Montgomery, D. R., and K. B. Gran (2001), Downstream variations in the width of bedrock channels, *Water Resour. Res.*, *37*, 1841–1846.

Montgomery, D. R., T. M. Massong, and S. C. S. Hawley (2003), Influence of debris flows and log jams on the location of pools and alluvial channel reaches, Oregon Coast Range, *Geol. Soc. Am. Bull.*, *115*, 78–88.

Moussavi-Harami, R., A. Mahboubi, and M. Khanehbad (2004), Analysis of controls on downstream fining along three gravel-bed rivers in the Band-e-Golestan drainage basin NE Iran, *Geomorphology*, *61*, 143–153.

Paola, C., G. Parker, R. Seal, S. K. Sinha, J. B. Southard, and P. R. Wilcock (1992), Downstream fining by selective deposition in a laboratory flume, *Science*, *258*, 1757–1760.

Parker, G., and P. C. Klingeman (1982), On why gravel bed streams are paved, *Water Resour. Res.*, *18*, 1409–1423.

Parker, G. (1990), Surface-based relation for bedload transport in gravel rivers, *J. Hydraul. Eng.*, *28*(4), 417–436.

Parker, G. (1991a), Selective sorting and abrasion of river gravel, I. Theory, *J. Hydraul. Eng.*, *117*, 131–149.

Parker, G. (1991b), Selective sorting and abrasion of river gravel, II. Applications, *J. Hydraul. Eng.*, *117*, 150–171.

Peizhen, Z., P. Molnar, and W. R. Downs (2001), Increased sedimentation rates and grain sizes 2–4 Myr ago due to the influence of climate change on erosion rates, *Nature*, *410*, 891–897, doi:10.1038/35073504.

Perfect, E. (1997), Fractal models for the fragmentation of rocks and soils: A review, *Eng. Geol.*, *48*, 185–198.

Pizzuto, J. E. (1995), Downstream fining in a network of gravel-bedded rivers, *Water Resour. Res.*, *31*, 753–759.

Posadas, A., D. Gimenez, M. Bittelli, C. M. P. Vaz, and M. Flury (2001), Multifractal characterization of soil particle-size distributions, *Soil Sci. Soc. Am. J.*, *65*, 1361–1367.

Reusser, L. J., P. R. Bierman, M. J. Pavich, E. Zen, J. Larsen, and R. Finkel (2004), Rapid late Pleistocene incision of Atlantic passive-margin river gorges, *Science*, *305*, 499–502.

Rice, S. (1998), Which tributaries disrupt downstream fining along gravel-bed rivers?, *Geomorphology*, *22*, 39–56.

Rice, S. (1999), The nature and controls on downstream fining within sedimentary links, *J. Sediment. Res., Sect. A*, *69*, 32–39.

Rice, S., and M. Church (1998), Grain size along two gravel-bed rivers: Statistical variation, spatial pattern and sedimentary links, *Earth Surf. Processes Landforms*, *23*, 345–363.

Rinaldo, A., I. Rodriguez-Itube, R. Rigon, E. Ijjasz-Vasquez, and R. L. Bras (1993), Self-organized fractal river networks, *Phys. Rev. Lett.*, *70*, 822–826.

Rinaldo, A., G. Vogel, R. Rigon, and I. Rodriguez-Iturbe (1995), Can one gauge the shape of a basin?, *Water Resour. Res.*, *31*, 1119–1127.

Rodriguez-Iturbe, I., and A. Rinaldo (1997), *Fractal River Basins: Chance and Self-Organization*, Cambridge Univ. Press, New York.

Schumm, S. A., and M. A. Stevens (1973), Abrasion in place: A mechanism for rounding and size reduction of coarse sediments in rivers, *Geology*, *1*, 37–40.

Sklar, L. S., and W. E. Dietrich (1998), River longitudinal profiles and bedrock incision models: Stream power and the influence of sediment supply, in *Rivers Over Rock: Fluvial Processes in Bedrock Channels*, *Geophys. Monogr. Ser.*, vol. 107, edited by K. J. Tinkler and E. E. Wohl, pp. 237–260, AGU, Washington, D. C.

Sklar, L. S., and W. E. Dietrich (2004), A mechanistic model for river incision into bedrock by saltating bedload, *Water Resour. Res.*, *40*, W06301, doi:10.1029/2003WR002496.

Sklar, L. S., and W. E. Dietrich (2006), The role of sediment in controlling bedrock channel slope: Implications of the saltation-abrasion incision model, *Geomorphology*, doi:10.1016/j.geomorph.2005.08.019, in press.

Stock, J. D., and W. E. Dietrich (2003), Valley incision by debris flows: Evidence of a topographic signature, *Water Resour. Res.*, *39*(4), 1089, doi:10.1029/2001WR001057.

Surian, N. (2002), Downstream variation in grain size along an Alpine river: Analysis of controls and processes, *Geomorphology*, *43*, 137–149.

Troutman, B. M., and M. R. Karlinger (1984), On the expected width function for topological random channel networks, *J. Appl. Probab.*, *22*, 836–849.

Troutman, B. M., and T. M. Over (2001), River flow mass exponents with fractal channel networks and rainfall, *Adv. Water Resour.*, *24*, 967–989.

Turcotte, D. L. (1997), *Fractals and Chaos in Geology and Geophysics*, 2nd ed., Cambridge Univ. Press, New York.

Venugopal, V., S. G. Roux, E. Foufoula-Georgiou, and A. Arneodo (2006), Revisiting multifractality of high-resolution temporal rainfall using a wavelet-based formalism, *Water Resour. Res.*, *42*, W06D14, doi:10.1029/2005WR004489.

Whipple, K. X. (2004), Bedrock rivers and the geomorphology of active orogens, *Annu. Rev. Earth Planet. Sci.*, *32*, 151–185.

Wilcock, P. R., S. T. Kenworthy, and J. C. Crowe (2001), Experimental study of the transport of mixed sand and gravel, *Water Resour. Res.*, *37*, 3349–3358.

Willis, C. M., and G. B. Griggs (2003), Reductions in fluvial sediment discharge by coastal dams in California and implications for beach sustainability, *J. Geol.*, *111*, 167–182, doi:10.1086/345922.

Wolkowinsky, A. J., and D. E. Granger (2004), Early Pleistocene incision of the San Juan River, Utah, dated with ^{26}Al and ^{10}Be, *Geology*, *32*, 749–752, doi:10.1130/G20541.1.

D. Bellugi and W. E. Dietrich, Department of Earth and Planetary Science, University of California, Berkeley, CA 94720, USA.

E. Foufoula-Georgiou and B. Lashermes, St. Anthony Falls Laboratory, 2 Third Avenue SE, Minneapolis, MN 55414, USA.

L. S. Sklar, Department of Geosciences, San Francisco State University, 1600 Holloway Avenue, San Francisco, CA 94132, USA. (leonard@sfsu.edu)